Journal of Environmental Radioactivity 257 (2023) 107078

Contents lists available at ScienceDirect

Journal of Environmental Radioactivity

journal homepage: www.elsevier.com/locate/jenvrad

Understanding deforestation impacts on soil erosion rates using ^{137}Cs, $^{239+240}Pu$, and $^{210}Pb_{ex}$ and soil physicochemical properties in western Iran

Maral Khodadadi [a,b,*], Christine Alewell [c], Mohammad Mirzaei [d], Ehssan Ehssan-Malahat [e], Farrokh Asadzadeh [e], Peter Strauss [f], Katrin Meusburger [g]

[a] Nuclear Agriculture Research School, Nuclear Science and Technology Research Institute (NSTRI), 31485/1498, Iran
[b] Department of Geology and Environmental Earth Science, Miami University, Oxford, OH, United States
[c] Environmental Geosciences, University of Basel, Bernoullistrasse 30, CH-4056, Basel, Switzerland
[d] Nuclear Science and Technology Research Institute (NSTRI), Karaj, 31485/1498, Iran
[e] Department of Soil Science, Urmia University, Urmia, 5756151818, Iran
[f] Institute for Land and Water Management Research, Federal Agency for Water Management, Pollnbergstrasse 1, A-3252, Petzenkirchen, Austria
[g] Swiss Federal Institute for Forest, Snow, and Landscape Research (WSL), 8903, Birmensdorf, Switzerland

ARTICLE INFO

Keywords:
^{137}Cs
$^{239+240}Pu$
$^{210}Pb_{ex}$
Soil organic carbon redistribution
Land-use change
Zarivar lake

ABSTRACT

To investigate the effects of converting forests into vineyards typical to Zarivar Lake watershed, Iran, which occurred mainly in the 1970s and 80s, on soil erosion, ^{137}Cs and $^{210}Pb_{ex}$, being mid-and-long-term soil loss tracers, were applied. In Chernobyl-contaminated areas like those found in some parts of Europe and Asia, the proportion of ^{137}Cs Chernobyl fallout needs to be determined to convert ^{137}Cs inventories into soil erosion rates. To do so, Pu radioisotopes were applied for the first time in Iran. The soil samples were gathered from two adjacent, almost similar hillslopes under natural forest (slope length: 250 m; slope gradient: 20%) and rainfed vineyard (slope length: 200 m; slope gradient: 17%). $^{137}Cs/^{239+240}Pu$ ratios indicated that 49.8 ± 10.0% of ^{137}Cs originated from Chernobyl. The net soil erosion rates derived by ^{137}Cs, and $^{210}Pb_{ex}$ approaches were 5.0 ± 1.1 and 5.9 ± 2.9 Mg ha^{-1} yr^{-1} in the forested hillslope, and 25.9 ± 5.7 and 32.5 ± 14.5 Mg ha^{-1} yr^{-1} in the vineyard hillslope, respectively. Both ^{137}Cs and $^{210}Pb_{ex}$ highlighted that deforestation increased soil erosion by around five times. Moreover, the impacts of deforestation on soil physicochemical properties were investigated in surface and subsurface soils. Compared to forested hillslope, soil organic carbon stock in the upper 40 cm of the vineyard reduced by 14 Mg C ha^{-1} (29%), 8 Mg C ha^{-1} of which was removed by erosion within 35 years, and the remaining have likely been lost via emissions (6 Mg C ha^{-1}). The vineyard topsoil experienced the most dramatic drops in percolation stability (PS), sealing index, and organic matter by about 55, 51, and 49%, respectively. Among all measured physicochemical properties, PS showed the greatest sensitivity to land-use change. Overall, the present study's findings confirmed that deforestation for agricultural purposes triggered soil loss, deteriorated soil quality and possibly contributed to the reduction of the lake's water quality and climate change.

1. Introduction

A rapidly growing population and a desire for a better standard of living have induced the need for intensive agricultural production in Iran, making the conversion from natural to cultivated lands inevitable. In fact, over the past 50 years, land-use changes in the country have occurred remarkably faster than in the previous century and are anticipated to accelerate in the future (Emadodin et al., 2012). Natural forests have shrunk from 19 million ha (11.5% of the total area of the country) in the 1950s to 12.4 million ha (7.5%) in the 1990s (DEI, Department of environment Iran, 2003), while cultivated land has expanded by more than seven times, from 2.6 million ha (1.6%; Wilber, 1948) to 18.5 million ha (11.2%; DEIDepartment of environment Iran, 2003). Meanwhile, around 2.5 million ha of Iran's agricultural land (1.5%) was converted to urban areas during the last decade, threatening food security. Consequently, deforestation and the cultivation of marginal lands, including fragile upland ecosystems, have become more prevalent in the country. Generally, land-use change on steep slopes is expected to

* Corresponding author. Nuclear Agriculture Research School, Nuclear Science and Technology Research Institute (NSTRI), 31485/1498, Iran.
E-mail address: khodadm@miamioh.edu (M. Khodadadi).

https://doi.org/10.1016/j.jenvrad.2022.107078
Received 13 June 2022; Received in revised form 8 November 2022; Accepted 17 November 2022
Available online 21 November 2022
0265-931X/Published by Elsevier Ltd.

influence soil erosion (Nunes et al., 2011; Zhang and Wang, 2017; Nabiollahi et al., 2018) and soil quality and health (Zeraatpisheh et al., 2020; Nabiollahi et al., 2018). Thus, to entirely understand deforestation impacts, soil erosion and soil physicochemical properties, including aggregate stability, should be investigated.

Fallout radionuclides (FRNs), largely Caesium-137 (^{137}Cs), unsupported Lead-210 (^{210}Pb$_{ex}$), and in recent years $^{239+240}$Pu, have been proven helpful in quantifying time-integrated estimates of medium-term (^{137}Cs and $^{239+240}$Pu ca. 50 yr) or long-term (^{210}Pb$_{ex}$ ca. 100 yr) soil redistribution rates (Meusburger et al., 2016). ^{137}Cs (half-life 30.2 years) is an anthropogenic isotope produced by atmospheric testing of thermonuclear weapons during the 1950s and 1960s (i.e., global fallout) or nuclear incidents like the one occurring in Chernobyl NPP in April–May 1986. In contrast, ^{210}Pb (half-life of 22.3 years) is a geogenic radionuclide, originated from the decay of gaseous ^{222}Rn, a daughter of ^{226}Ra (Mabit et al., 2008). A fraction of ^{222}Rn produced from the lithogenic sources escapes and produces ^{210}Pb, which is then precipitated on the soil surface. This deposition is called "excess" or "unsupported" ^{210}Pb (^{210}Pb$_{ex}$), not being in equilibrium with its parent ^{226}Ra, and thus, able to be exploited as a soil redistribution tracer.

Generally, the worldwide pattern of globally derived ^{137}Cs fallout indicates that inputs are ranged between 160 and 3200 Bqm^{-2} (decay corrected to 1996) depending on latitude (UNSCEAR, 1969; Garcia Agudo, 1998). To estimate soil redistribution rates using ^{137}Cs measurements, additional ^{137}Cs fallout inputs, such as the Chernobyl accident, need to be considered. To convert ^{137}Cs inventories to soil erosion rates in the Chernobyl-contaminated areas, the proportion of ^{137}Cs Chernobyl fallout must be determined (Meusburger et al., 2018). To quantify the relative proportion of Chernobyl fallout to the total ^{137}Cs inventory, plutonium (Pu) radioisotopes have recently been suggested (Alewell et al., 2017) and applied successfully.

The two major anthropogenic radioisotopes of Pu, i.e., ^{239}Pu [half-life of 24 110 - years] and ^{240}Pu [half-life of 6561 years], are alpha-emitting actinides coming from nuclear weapon tests, nuclear weapon manufacturing, nuclear fuel reprocessing, and nuclear power plant accidents (Ketterer and Szechenyi, 2008). Globally, it was observed that the Pu 1950s–60s fallout is almost identical to that of ^{137}Cs distribution (Alewell et al., 2014). Nonetheless, unlike ^{137}Cs, Pu is found in the non-volatile fraction of nuclear fuel debris originated from reactor incidents like the one in Chernobyl. Hence, specific regions of Russia, Belarus, Ukraine, the Baltic countries, Poland, and Scandinavia were the geographic zones over which Pu Chernobyl fallout was deposited (Mietelski and Was, 1995). If Pu exclusively comes from global fallout, the ratio of Pu to Cs isotopes can reveal whether the area received Chernobyl ^{137}Cs deposition (Schaub et al. (2010); Alewell et al. (2014); Meusburger et al., 2020).

Conversion of natural vegetation to farmland can alter soil properties, and these changes may further enhance soil erosion. An important factor in soil resistance to erosion is aggregate stability (Auerswald, 1995). Percolation Stability (PS) is a suitable method to assess aggregate stability (Mbagwu and Auerswald, 1999), with the advantage of being less labor intensive than the wet sieving method. Through rapid wetting, PS calculates the resistance of aggregates against slaking, thus triggering numerous subprocesses of erosion (Auerswald, 1995). Also, crusts contribute to runoff and soil erosion (Valentin and Bresson, 1997; Fageria et al., 2010). The crust formation is associated with low organic matter (OM) content and a high percentage of silt (Valentin and Bresson, 1997). Since monitoring permeability and soil aggregate stability is often time-consuming and expensive, various indices were developed to predict soil crusting using more available data like soil texture and organic matter content (Udom and Kamalu, 2016).

Despite relatively high inventories of ^{137}Cs reported in the north of Iran (Vahabi-Moghaddam and Khoshbinfar, 2012; Gharibreza et al., 2020), the origin and relative contribution of these types of fallout have not been established. Thus, the present study was undertaken to quantify the impacts of deforestation on soil loss and soil physicochemical properties in a Chernobyl-contaminated region typical of deforestation on steep slopes. The objectives of this study were (i) to estimate the proportion of ^{137}Cs Chernobyl input using $^{239+240}$Pu in the study site, (ii) to quantify soil redistribution rates using ^{137}Cs and ^{210}Pb$_{ex}$ in two adjacent hillslopes under different land uses, and (iii) to evaluate the effects of deforestation on soil loss and soil physicochemical properties.

2. Materials and methods

2.1. Study area

To study the effects of deforestation on soil physicochemical properties and soil erosion rates on steep slopes, Zarivar Lake watershed, Kurdistan Province, northwest of Iran, was chosen. The watershed is located in Zagros forests, known as western oak forests, in the Zagros Mountains. Converting the steep hillslopes naturally under oak forest to rainfed vineyards has been one of the most common land-use changes in the area. Zarivar Lake (35° 33' 15″ N and 46° 7' 25" E) is a shallow freshwater reservoir located 3 km northwest of Marivan city, Kurdistan Province, Iran (Fig. 1a). The lake drains an area of about 296.4 km^2. The landscape in this region is characterized by mountains covered by deciduous oak forests, hills extensively covered by vineyards, and plains used mainly for cereal cultivation.

The average annual precipitation and air temperature are 991.2 mm and 12.8 °C, respectively (Iran Meteorological Organization). "Z3" subwatershed, with a total area of about 2.97 km^2 and an average altitude of 1518 m a.s.l. (ranging from 1292 to 1876 m a.s.l.) was selected for this study. The parent materials in ridges are metamorphic rocks of complexly folded black shale and minor metamorphosed limestone and sandstones, while in the lowlands, they consist of Quaternary sediments, mainly, lacustrine deposits (Geological survey and mineral exploration of Iran). According to soil taxonomy, the soils of the watershed are categorized as Typic Haploxeralfs and Typic Haploxerepts (Soil Taxonomy, 2014).

Two adjacent hillslopes with different land uses were selected to collect samples. One was under natural forest (slope gradient: 20%; slope length: 250 m; exposure: East), whereas the other was deforested in 1981 and converted to a rainfed vineyard (slope gradient: 17%; slope length: 200 m; exposure: East). The hillslopes were selected having almost similar slope gradients, length, and exposures (Fig. 1a). The forest is an open forest type, and understory plants typically present a high degree of cover (up to 100%), while in the vineyard, the soil between the vines is bare.

2.2. Soil redistribution rates using FRNs

2.2.1. Soil sampling design

FRNs as soil erosion tracers are used by comparing their inventories in sites affected by soil redistribution processes with their baseline inventory at a reference site (Mabit et al., 2008, 2012). A crucial step that should be taken when using FRN techniques is to find an undisturbed reference site (Mabit et al., 2008, 2012). Here, a flat undisturbed site under perennial grass, located in relatively vast areas without trees, was selected. This reference site, with an elevation of 1397 m, is situated ca. 800 m far from the study sites (Fig. 1a). The site was selected following the IAEA's (2014) guidelines, suggesting an acceptable radius of around 1 km. In the literature, there have been numerous cases with similar or farther distances, e.g., Mabit and Bernard (2007): 0.5 km, Mabit et al. (2009): 1 km radius, Abbaszadeh Afshar et al. (2010): <1 km, Lal et al. (2013): 20 km radius, and Alewell et al. (2014): >1 km. Eleven bulk samples were collected to calculate the initial inventory of FRNs at the reference site. For collecting samples, manual soil column cylinder augers were designed and built. A sectioned core was collected at 2 cm increments using a scraper plate sampling device (50 cm × 20 cm) designed by Campbell et al. (1988).

At the two studied hillslopes, a multi-transect sampling approach

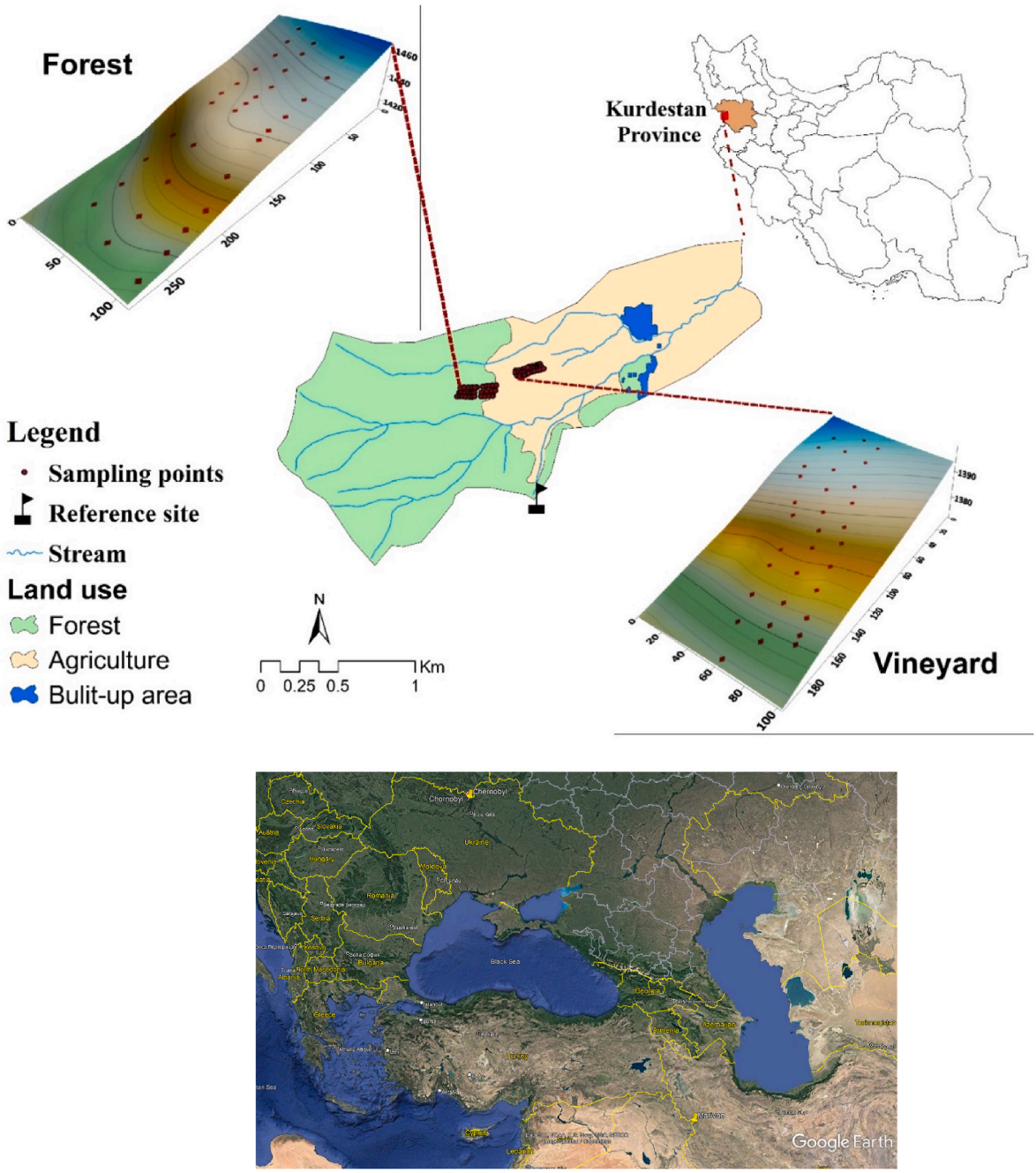

Fig. 1. The location of the Z3 sub-watershed in Kurdistan Province and Iran, the reference site, and the study hillslopes and sampling points (a), and the location of the study site relative to the Chernobyl NPP.

Table 1
Number and type of samples collected at reference, forested, and vineyard sites.

Site	Number soil of samples for FRN measurements	Depth (cm)	Number soil of samples for physicochemical property measurements	Depth (cm)
Reference	Increment sample:15	2		
	Bulk sample: 11	30		
Forest	Increment sample: 6	5	6	0–20
	Bulk sample: 33	30	6	20–40
Vineyard	Increment sample: 8	5	7	0–20
	Bulk sample: 33	40	7	20–40

was adopted. In each site, a total of 33 bulk soil cores were collected along three parallel transects in the main slope direction (Table 1; Fig. 1a). Soil sampling was performed up to 30 and 40 cm depths in forested and vineyard hillslopes, respectively. To ascertain that all FRN in the soil profile was sampled in locations where the deposition was expected, the samples were collected up to 40 and 50 cm in forested and vineyard hillslopes, respectively, whenever the soil was deep enough. A sectioned core at 5 cm increments was also collected in an erosional site in each hillslope (at the second or third sampling point of the middle transect).

2.2.2. *Soil sample pre-treatment and radioisotopic analysis*

Soil samples were air-dried, disaggregated, sieved to <2 mm, ground, and then homogenized. Soil samples were analyzed for ^{137}Cs

and ^{210}Pb, and ^{226}Ra by gamma spectrometry using an N-type HPGe detector. The calibration accuracy was established using IAEA reference materials (Soil 6 and Soil 375). Gamma spectrometry measurements were undertaken in the Iranian Nuclear Medicine Research Institute. Before analyzing ^{210}Pb, sub-soil samples were sealed for one month to achieve equilibrium between ^{226}Ra and its daughter ^{214}Pb. ^{137}Cs, total ^{210}Pb, and ^{214}Pb activities were established from the net peak areas of gamma rays at 661.6, 46.5, and 352 keV, respectively. To reach a precision of maximum 20% at the 95% confidence level, counting times ranged between 12 and 24 h.

To determine the proportion of ^{137}Cs Chernobyl fallout in the samples, 39 bulk and increment samples were selected for $^{239+240}$Pu measurement, including reference bulk samples, reference increment samples, a transect in the forest, and increment samples of an erosional site. Noteworthy is that the primary aim of measuring $^{239+240}$Pu was to quantify the proportion of ^{137}Cs Chernobyl fallout. Thus, to prioritize the limited funding available, we did not measure $^{239+240}$Pu in the rest of the samples. According to the method explained by Ketterer et al. (2012), the samples were prepared for the analysis of Plutonium isotopes. Plutonium isotopes were measured with a Thermo X Series II quadrupole ICP-MS instrument, coupled with a high-efficiency dissolving sample introduction system, at the University of Cadiz, Spain. The measurement error was 1–3%, with the detection limit of 0.1 Bq kg^{-1}. Existing ^{239}Pu and ^{240}Pu masses in the sample (which were indicated by isotope dilution calculation) were presented as the aggregated $^{239+240}$Pu activity to correspond with alpha spectrometric measurements of Pu activity. The ^{240}Pu/^{239}Pu atom ratios were distinguished through the same analytical run. The quality of measurements was assessed by analyzing preparation blanks (soils or rocks bereft of Pu), control samples, and duplicates with pre-determined $^{239+240}$Pu activities.

Cultivation history, i.e. if the soils have been disturbed, must be taken into account when selecting conversion models used to convert FRN inventories to soil redistribution rates (Walling et al., 2002, 2014). This distinction has to be made due to different FRN profiles in cultivated and uncultivated soils. While FRNs are almost uniformly distributed through plow layer in the former, they are expected to accumulate mostly closer to the surface in the latter. This means a decrease in FRN concentrations indicates far higher rates of erosion in cultivated lands rather than in uncultivated ones (Walling et al., 2014). Thus, to estimate soil redistribution rates, two models, i.e., the Diffusion and Migration Model (DMM) (Walling et al., 2002, 2014), and Modelling Deposition and Erosion rates with RadioNuclides (MODERN; Arata et al., 2016a,b) in forested hillslope were used, while in cultivated hillslope, Mass Balance Model II (MBM II) was applied (Walling et al., 2002, 2014). It is noteworthy that MODERN does not consider the progressive dilution of FRN concentrations within the plow layer, so it was not used at the vineyard. Indeed, in cultivated areas, there is a progressive dilution of FRN concentrations due to incorporating soil from below the original plow depth to compensate for the depth lost by erosion (IAEA, 2014). In order to propagate errors for the estimated soil erosion rates, we employed the following method. Given there are two sources of uncertainty, uncorrelated to one another, namely the uncertainty of measurements ($S_{\bar{x}}$) and the CVs of FRNs at the reference site ($S_{\bar{y}}$), the standard errors ($S_{\bar{z}}$) were propagated using equation (1). equation (1) results were multiplied by the estimation of the conversion models, resulting in a confidence interval for each FRN.

$$S_{\bar{z}} = \sqrt{(S_{\bar{x}})^2 + (S_{\bar{y}})^2} \tag{1}$$

The maps of soil redistribution rates were created using the spatialization module of Inverse Distance Weighting power 2 (IDW2) in Surfer software package 16.0. IDW employs a weighted average interpolation technique assigning greater weight to adjacent points, making the weights inversely proportionate to the power of the distance (Oliver and Webster, 2015).

2.3. Soil sampling and soil physicochemical properties

Soil samples were collected along transects at six and seven points in the vineyard and forested hillslope, respectively (Table 1). Samples were gathered from two depths of 0–20 and 20–40 cm. The samples were air-dried, disaggregated, and sieved to <2 mm. Soil pH (McLean et al., 1982) and electric conductivity (ECe) (Rhoades, 1982) were indicated in the saturated paste and saturated paste extract, respectively. Soil texture, or particle size distribution (PSD) (wet sieving and pipette method, Gee and Bauder, 1986), and bulk density (BD) (core method; Blake and Hartge, 1986) were measured. Porosity (f) of the soils was calculated using soil bulk density (Danielson and Sutherland, 1986). The soil moisture at field capacity (FC) and the wilting point (PWP) were gauged by a pressure plate apparatus (Klute, 1986) at 33 and 1500 kPa, respectively. The available water capacity (AWC) was calculated by subtracting PWP from FC. Percolation stability was measured in a laboratory test with air-dried 1–2 mm aggregates (Siegrist et al., 1998) at the Federal Agency for Water Management Austria, Vienna, Austria. In this method, the water is percolated through a small plexiglass tube filled with a sample with a constant hydrostatic head. The amount of percolated water during 600s was used to calculate PS values.

Soil organic carbon (SOC) (Walkley-Black method; Nelson and Sommers, 1982), carbonate calcium equivalent (CCE) (Jackson, 1958) and cation exchange capacity (CEC) (determined using Rhoades, 1982 method) were also measured using standard methods. Total nitrogen (TN) was measured by Kjeldahl method (Bremner, 1996). The SOC concentration derived by the TN concentration generates the soil C:N ratio. The soil organic carbon stock (SOCS) was computed with the equation proposed by Hiederer and Köchy (2011). Soil permeability was measured using double-ring infiltrometers, and a soil profile was also studied in each hillslope (Scholten, 1997).

The soil erodibility (K) factor was estimated using Wischmeier and Smith (1978). The equation considers the OM content, aggregate stability, infiltration rate, and PSD. To assess soil's susceptibility to crusting, soil physical quality indices were also computed, which included sealing index (SI) (Valentin and Bresson, 1997) and crusting index (CI) (FAO, 1978) using equation 2, and 3, respectively.

$$SI = \frac{OM \times 100}{Silt + Clay} \tag{2}$$

The value of the SI is regarded as high crusting or sealing risk if it is lower than 5%, whereas a value of more than 9% indicates a low sealing risk, and 7% is described as the threshold value (Udom and Kamalu, 2016).

$$CI = \frac{1.5(\%fine\ Silt + 0.75 coarse\ Silt)}{\%Clay + 10(\%OM)} \tag{3}$$

The values over 1.6 for CI represent that soils are prone to intense crusting, whereas values below 1.2 imply low crusting risk.

A statistical comparison between the topsoil and subsoil properties of the two land-use types was done by one-way analysis of variance (ANOVA). In fact, the H-value of the Kruskal–Wallis test offers a metric to evaluate the discriminatory power of a property between different classes (Berthon et al., 2011). Properties with higher H-values have higher discrimination powers (Berthon et al., 2011). The H-value was, thus, applied to compare the discrimination power of the significantly different properties of topsoil and subsoil classes between two land-use types, enabling the identification of the most sensitive properties to deforestation. SPSS software ver. 22 (IBM, Armonk, NY, USA) was employed to carry out all statistical analyses.

3. Results

3.1. Assessment of soil redistribution rates estimated by FRNs

3.1.1. FRN baseline inventories and ^{137}Cs chernobyl fallout proportion at the reference site

The depth profiles at the reference site of three FRNs showed an exponential decrease with depth (Fig. 2). The upper 12 cm of the soils contained 91.5%, 91.7%, and 90.4% of the ^{137}Cs, $^{239+240}$Pu, and ^{210}Pb$_{ex}$ inventory, respectively. The mean reference inventory values of ^{137}Cs, ^{210}Pb$_{ex,}$ and $^{239+240}$Pu were estimated to be 6152 ± 1266, 6079 ± 151, and 135 ± 31 Bq m^{-2}, respectively (Fig. 3).

The ^{137}Cs value obtained in our reference site was higher than most values reported for reference inventories in Iran (Table 2). Therefore, it was hypothesized that the study site possibly received Chernobyl-derived ^{137}Cs fallout (Fig. 1b). Lawrence Livermore National Laboratory map shows that the radioactive Chernobyl cloud reached west of Iran on 6 May 1986 (users.owt.com). Foucher et al. (2021) also indicated that the Northwest of Iran was contaminated by the Chernobyl fallout. The CHELSA (Climatologies at high resolution for the earth's land surface areas) dataset (Karger et al., 2017) confirmed that the study site received around 150 and 100 mm rainfall in April and May 1986, respectively.

At our reference site, the average atomic ratio of ^{240}Pu/^{239}Pu was 0.184 ± 0.020, ranging from 0.121 to 0.262 (Fig. 4). Here, to determine the proportion of the ^{137}Cs Chernobyl input, the mean activity ratio of ^{137}Cs/$^{239+240}$Pu from global originated fallout was employed using the value reported by Hodge et al. (1996) at 38.4 (as of 1 July 1994) after values being decay-corrected to 1.10.2016, this amount reduces to 22.9. The Chernobyl-derived ^{137}Cs was calculated by subtracting the global inventory contribution from the reference site inventories (including global and Chernobyl fallout). The ^{137}Cs Chernobyl input in the study site was estimated to be 49.8 ± 10.0%.

3.1.2. Fallout radionuclides inventories and soil redistribution rates at slope transects

The mean and standard deviation of $^{239+240}$Pu inventory was 130.9 ± 54.5 Bq m^{-2} at the forested hillslope. ^{137}Cs inventories were 5389.9 ± 2227.9 and 4646.6 ± 1921.8 Bq m^{-2}, and ^{210}Pb$_{ex}$ inventories were 4068.3 ± 2345.8 and 3990.1 ± 2892.2 Bq m^{-2}, respectively for forested

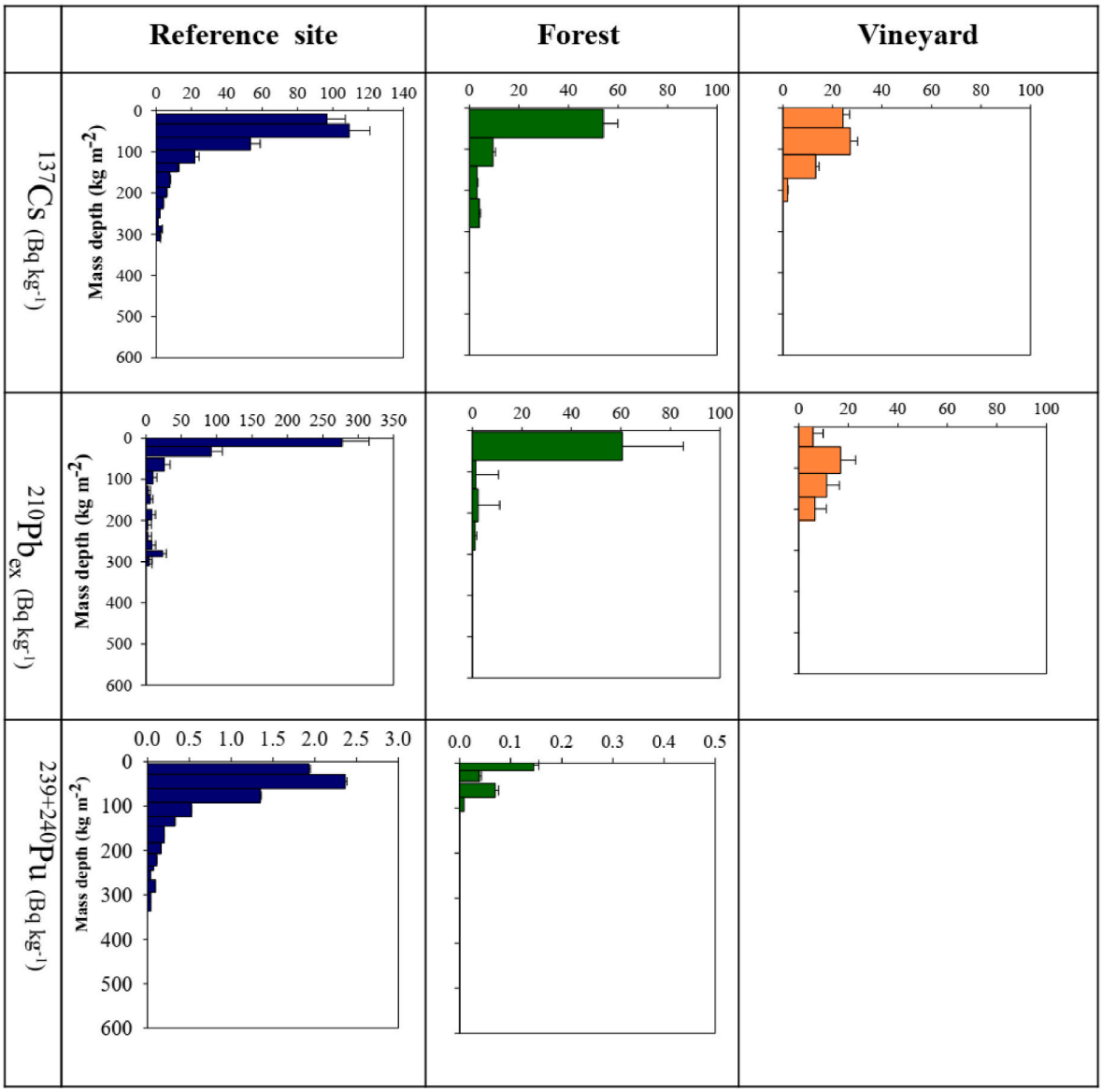

Fig. 2. Depth distribution of ^{137}Cs, ^{210}Pb$_{ex,}$ and $^{239+240}$Pu activities at the reference site and an erosional site in the forested and vineyard hillslopes. Scales are different on the x-axis.

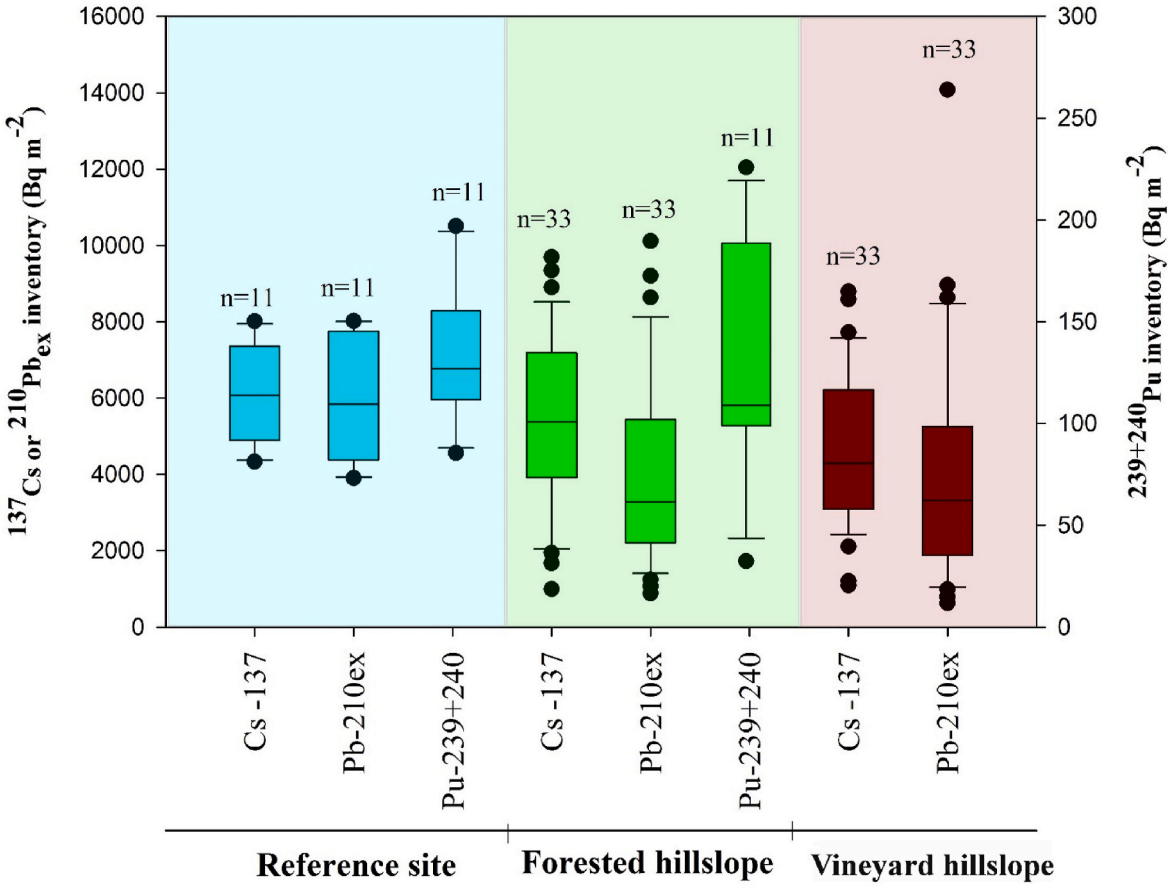

Fig. 3. ^{137}Cs, ^{210}Pb$_{ex}$, and $^{239+240}$Pu inventories at reference, forested, and vineyard sites (the scale of Y axes for ^{137}Cs and ^{210}Pb$_{ex}$ is different from that of $^{239+240}$Pu).

Table 2
^{137}Cs baseline inventory and mean annual precipitation (MAP) in undisturbed locations in different parts of Iran (all values were decay corrected to 1/10/2016).

Location	Mean Annual Precipitation (mm)	^{137}Cs inventory at reference site (Bq m^{-2})	Reference
Kouhin, centre of Iran	330	1956 ± 107	Khodadadi et al. (2018)
Aghemam Catchment, North-East of Iran	482	2714	Seyedalipour et al. (2014)
Rimeleh catchment, west of Iran	696	1544	Kalhor (1998); Matinfar et al. (2013)
Chaharmahal and Bakhtiari Province, West-South of Iran	600	1730 ± 32	Afshar et al. (2010)
Gorgan River watershed, North of Iran	562	2178	Shahoei and Rafahi (1998)
Golestan Province, North of Iran	700–1000	3840–4062	Gharibreza et al. (2020)
Gilan Province, North of Iran	1000	3570 -5270*	Vahabi-Moghaddam and Khoshbinfar (2012)
	1209	6180	Gharibreza et al. (2021)
Zarivar lake watershed, North-West of Iran	991	6152 ± 1266	This study

* Not all reported values were related to a reference site.

and vineyard hillslopes (Fig. 3). The average inventories of both ^{137}Cs and ^{210}Pb$_{ex}$ in the vineyard hillslope were moderately lower than those of the forested site. The coefficients of variation of ^{137}Cs, ^{210}Pb$_{ex,}$ and $^{239+240}$Pu for 11 bulk samples at the reference site were 21, 23, and 25%, respectively. The values were within the acceptable threshold for using FRN techniques, i.e., <30% (IAEA, 2014).

The sectioned profiles of ^{137}Cs, ^{210}Pb$_{ex,}$ and $^{239+240}$Pu in an erosional site in the second transect (mid-transect) of forested hillslope were compared (Fig. 2). Inventory changes in sectioned profiles of FRNs verified the dominance of soil erosion at the site, albeit having comparatively different values (Fig. 2). In other words, while inventory changes of ^{137}Cs and ^{210}Pb$_{ex}$ (−17 and −23%, respectively) were quite identical, the inventory change of the $^{239+240}$Pu (−86%), was notably high (Fig. 2). Supposedly, changes in microtopography of the hillslope over time might have brought about such discrepancies in FRN inventories. Depth distribution of ^{137}Cs and ^{210}Pb$_{ex}$ at an erosional vineyard site confirmed that an erosion process has occurred on the site (Fig. 2). Yet, ^{210}Pb$_{ex}$ showed a higher rate of soil erosion.

The average errors of soil erosion rates for ^{137}Cs and ^{210}Pb$_{ex}$ were calculated using equation (1). CVs of ^{137}Cs, $^{239+240}$Pu, and ^{210}Pb$_{ex}$ at the reference site were 21, 23, and 25%, respectively, and the average uncertainty of measurements were 5, 1, and 22%, respectively, resulting in 21.6, 23.0, and 33.3%, in respective order after being introduced to equation (1). Finally, the confidence intervals of the soil erosion rates were calculated by converting the upper and lower inventories within the error range. At the forested hillslope, the net soil erosion rate estimated by MODERN for ^{210}Pb$_{ex}$ (5.9 ± 1.1 Mg ha^{-1} yr^{-1}) was slightly more than that of ^{137}Cs (5.0 ± 2.5 Mg ha^{-1} yr^{-1}) and $^{239+240}$Pu (1.7 ± 0.4 Mg ha^{-1} yr^{-1}); subsequently, respective SDRs of 96, 70 and 66% were computed (Table 3). By contrast, the ones estimated by DMM were considerably different for these two FRNs, with 2.0 and 5.1 Mg ha^{-1} yr^{-1}

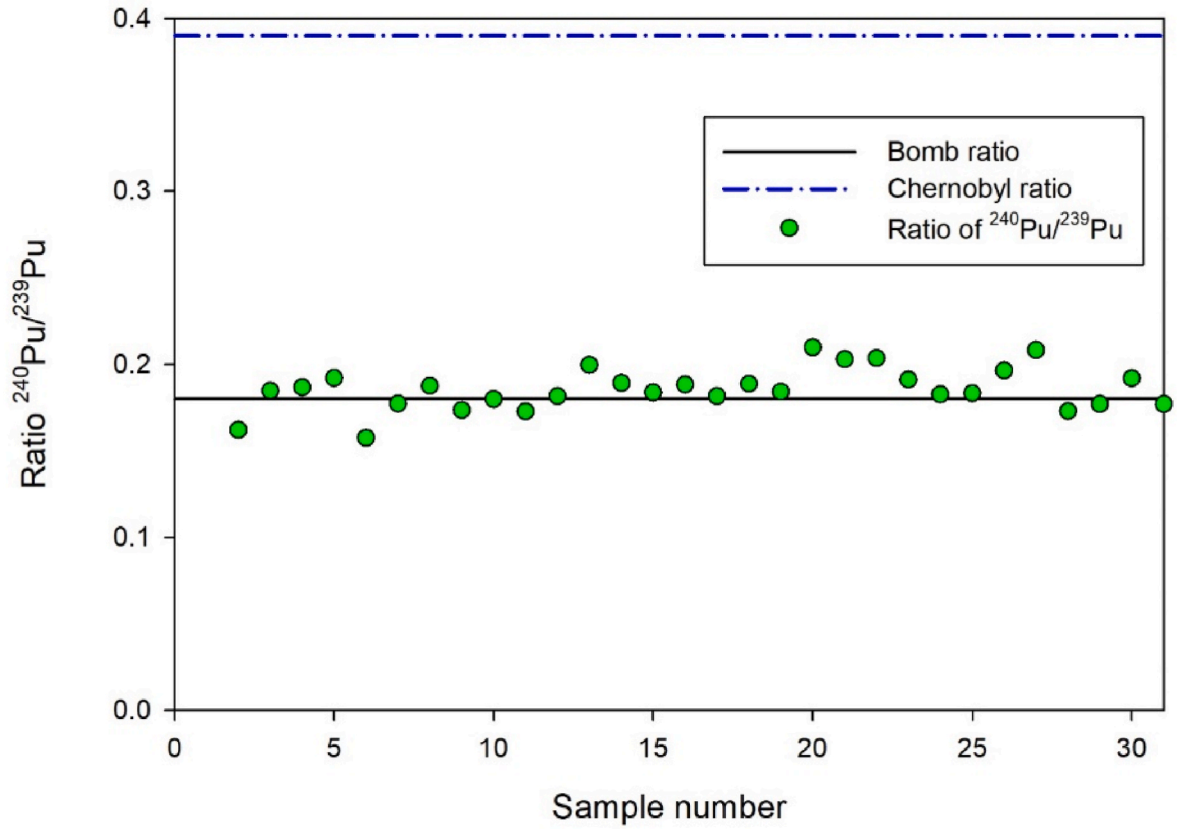

Fig. 4. The ratio of $^{240}Pu/^{239}Pu$ of samples at the reference site and the forested hillslope.

Table 3
Sediment budget based on ^{137}Cs and $^{210}Pb_{ex}$ dataset at forest and orchard sites.

Sediment budget	Forect					Vineyard	
	^{137}Cs		$^{210}Pb_{ex}$		$^{239+240}Pu$	^{137}Cs	$^{210}Pb_{ex}$
	MODERN	DMM	MODERN	DMM	MODERN	MBM II	
Net erosion (Mg ha^{-1} yr^{-1})	5.0 ± 1.1	2.0 ± 0.4	5.9 ± 2.0	5.1 ± 1.7	1.7 ± 0.4	25.9 ± 5.7	32.5 ± 10.8
Sediment Delivery Ratio (%)	69.9	83.0	95.9	92.8	65.5	95.2	91.9

for ^{137}Cs and $^{210}Pb_{ex}$, respectively. At the vineyard hillslope, the net soil redistribution rates estimated by MBM II were 25.9 ± 5.7 and 32.5 ± 14.5 Mg ha^{-1} yr^{-1}, respectively, which was about five times more than those at the forested hillslopes. Consequently, SDRs were estimated to be around 95 and 92% for ^{137}Cs and $^{210}Pb_{ex}$, respectively (Table 3). In general, SDRs calculated in both hillslopes using different models were extremely high, indicating that most of the eroded soil was removed from the hillslopes. The correlation between inventories of $^{210}Pb_{ex}$ and $^{239+240}Pu$ with ^{137}Cs along a transect in forested hillslope was examined (Fig. 5a). A stronger positive correlation was observed between ^{137}Cs and $^{239+240}Pu$ (ca. $r^2 = 0.82$) than between ^{137}Cs and $^{210}Pb_{ex}$ (ca. $r^2 = 0.56$). Also, the soil redistribution rates of the three FRNs in the forested transect were estimated using the MODERN and DMM (Fig. 6b). While DMM estimated soil losses for $^{210}Pb_{ex}$ were higher than those of ^{137}Cs in most sampling points, MODERN estimated soil losses and gains for $^{239+240}Pu$ were by far the highest along the transect (Fig. 5b).

Soil redistribution rates estimated by ^{137}Cs and $^{210}Pb_{ex}$ followed relatively similar patterns in both sites (Fig. 6). Although both radionuclides indicated soil loss was the dominant process in both hillslopes, the magnitude of soil loss in the vineyard site was several times higher than those in the forested site (Fig. 6). In the vineyard site, the soil redistribution pattern of both radionuclides showed that deposition had occurred mainly along the third transect, which was expected due to its gentle lateral slope (Fig. 6a and b). In the forested site, deposition happened in mid-slope, having a relatively lower slope gradient; however, due to the high slope gradient at the bottom of the slope (Fig. 6c and d), soil loss was the predominant process. Owing to the consistency between the estimated soil distribution rates and the topography features, both ^{137}Cs and $^{210}Pb_{ex}$ radionuclides proved valid in quantifying soil loss.

3.2. Assessment of soil physicochemical properties in the vineyard and forested hillslopes

Deforestation and land-use change from natural vegetation to agriculture have significantly increased ECe, pH, BD, and the K factor, while considerably decreasing OM, TN, C:N, CEC, AWC, *f*, and PS in surface soil (Table 4). Likewise, in the subsurface soils of two land-use types, there was a substantial rise in pH, BD, and K, yet a notable decline in clay, OM, TN, C:N, CEC, AWC, *f*, and PS (Table 3).

OM and TN in both depths were reduced in the vineyard compared to the forest; however, this reduction was greater in the surface layer (Table 4). The average OM content of the forest's topsoil is twice as high as the dry farming vineyard, i.e., 2.8 and 1.4% (Table 4), which

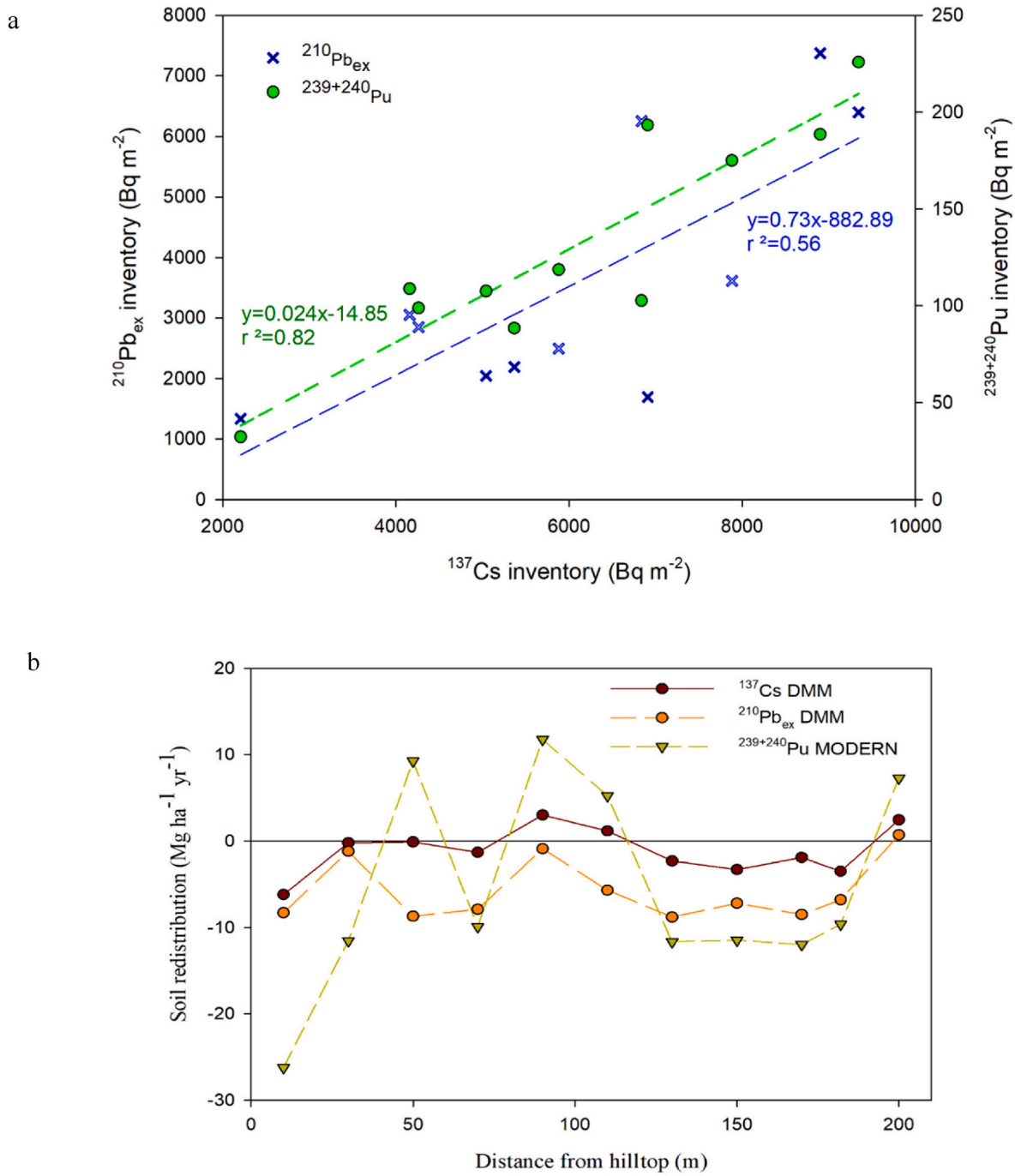

Fig. 5. Comparison of $^{210}Pb_{ex}$ and $^{239+240}Pu$ with ^{137}Cs inventories (a) and FRNs derived soil redistribution rates using MODERN and Diffusion and Migration model (DMM) (b) along a transect in the forested hillslope (negative values indicate erosion, whereas positive values indicate deposition).

correspond to a SOCS of 28.8 and 19.8 Mg ha^{-1}, respectively. Similarly, the OM contents in forest and vineyard subsoils were 1.7 and 1.2%, respectively, indicating a SOCS of 19.5 and 15.2 Mg ha^{-1}, respectively. The C:N ratio dropped with depth in both soils, most probably due to lower OM turnover (Table 4). Moreover, the BD of the vineyard topsoil was significantly greater than that of the forest (1.09 kg m^{-3} and 1.37 kg m^{-3} in the forest and vineyard topsoil, respectively) (Table 4). Similarly, following deforestation, the porosity of the surface and subsurface soils under the vineyard declined by around 11 and 10%, respectively.

Mbagwu and Auerswald (1999) classified PS into three classes, namely, rapid (>250 gr H_2O 600s^{-1}), moderate (250-150 gr H_2O 600s^{-1}), and slow (<150 gr H_2O 600s^{-1}). PSs were approximately 309 and 160 gr H_2O 600s^{-1} in forest and vineyard topsoil, in turn, falling into rapid and moderate categories, respectively. Rapid PS in forest soils is interpreted as high aggregate stability reflecting the higher OM content, but moderate PS in vineyard soils is an indicator of their weak structure. Furthermore, two indices were calculated to evaluate the surface crusting risk. The SI in all soil samples was less than 5%, indicating a high risk of sealing. CI in both topsoil and subsoil of the forest showed a low sealing risk (<1.2), while it was considered to have a moderate sealing risk in surface and subsurface soils of the vineyard (1.2–1.6). K-values in forest surface and subsurface soils were 0.044 and 0.054 t ha hr MJ^{-1} ha^{-1} mm^{-1}, respectively, whereas respective values for surface and subsurface vineyard soils were 0.051 and 0.067 t ha hr MJ^{-1} ha^{-1} mm^{-1} (Table 4).

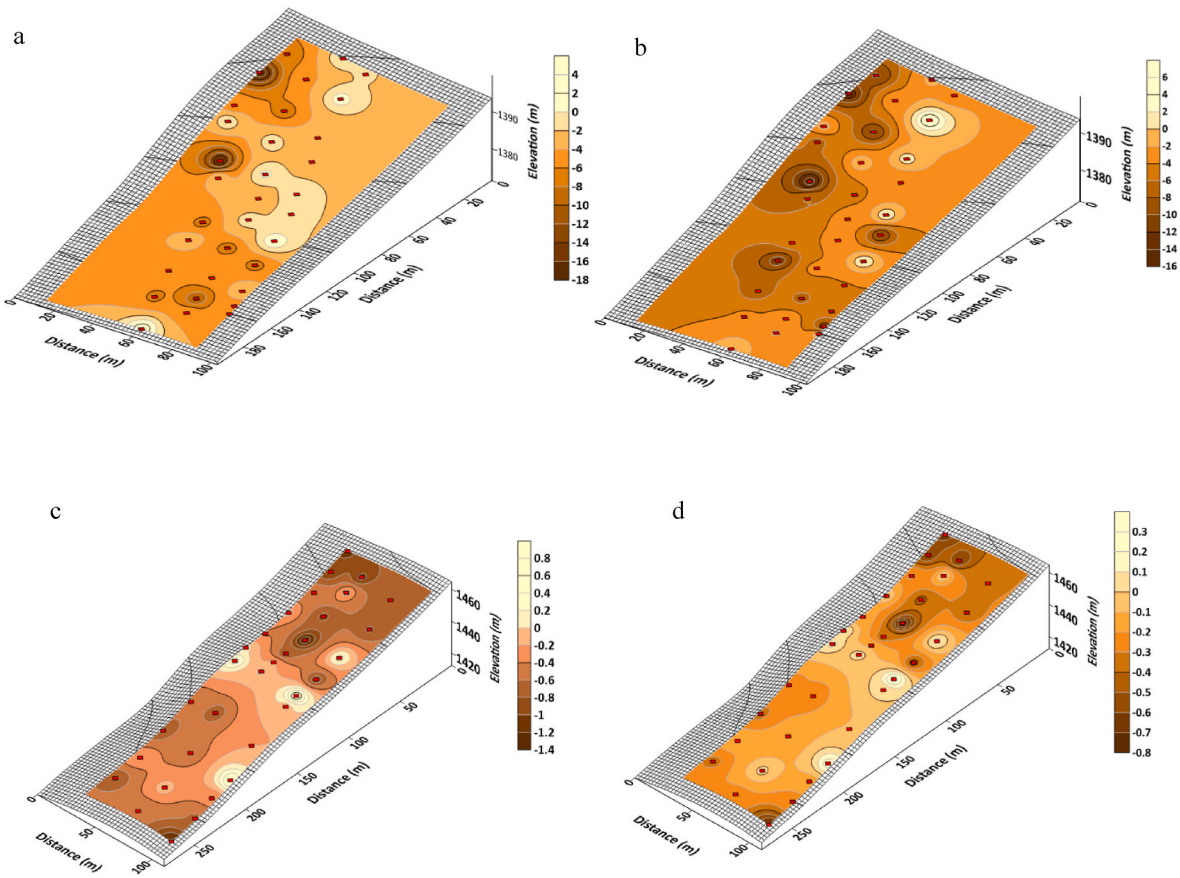

Fig. 6. Maps of soil redistribution rates (kg m^{-2} $year^{-1}$) derived by ^{137}Cs (a) and $^{210}Pb_{ex}$ (b) at the vineyard site, and by ^{137}Cs (c) and $^{210}Pb_{ex}$ (d) at the forested site using IDW2.

4. Discussion

4.1. Assessment of soil redistribution rates estimated by FRNs

4.1.1. FRN baseline inventories and ^{137}Cs chernobyl fallout proportion in the study area

The $^{240}Pu/^{239}Pu$ atom ratio of global fallout in mid-latitudes of the Northern Hemisphere is 0.180 ± 0.014 (Kelley et al., 1999), while the ratio of Chernobyl fallout is between 0.37 and 0.41 (Muramatsu et al., 2000; Ketterer et al., 2004). Thus, our measured $^{240}Pu/^{239}Pu$ ratios (with an average of ca 0.184 ± 0.020) are in accordance with the Kelly et al.'s (1999) atmospheric fallout value, implying that Pu solely originates from the global atmospheric fallout (Fig. 4). Thus, Pu could be used to quantify the proportion of the ^{137}Cs Chernobyl input, estimated to be 49.8 ± 10.0%. Substantial rainfall amounts after the Chernobyl incident (CHELSA dataset; Karger et al., 2017) also confirmed that the study site had been contaminated by Chernobyl-derived ^{137}Cs fallout.

Our mean reference inventory value of ^{137}Cs in the northwest of Iran (at 6152 ± 1266 Bq m^{-2}) was compatible with those observed in the Northeast of Iran, at 4000 Bq m^{-2} (Gharibreza et al., 2020), and in the north of Iran, at around 4420 (Vahabi-Moghaddam and Khoshbinfar, 2012) and 6180 Bq m^{-2} (Gharibreza et al., 2021) (Table 1). Overall, a relatively strong correlation was observed between ^{137}Cs inventories and MAP in the country ($r^2 = 0.72$; Fig. 7). For the site in the north of Iran investigated by Vahabi-Moghaddam and Khoshbinfar (2012), with similar MAPs, the ^{137}Cs inventories were reported to vary between 3570 and 5270 Bq m^{-2} moderately lower than our reported value. This can be due to a 400-km distance between the two sites and, more importantly, the fact that not all reported values were related to a well-defined reference site, meaning that the collected samples might have experienced soil redistribution.

The mean reference inventory value of $^{210}Pb_{ex}$ stood at 6079 ± 1511 Bq m^{-2}, which was moderately greater than the reported value in central Iran, at 5825 ± 297 Bq m^{-2}, with MAP of 330 mm (Khodadadi et al., 2018). The annual deposition flux of $^{210}Pb_{ex}$ was 205 Bq m^{-2} yr^{-1} for the region, falling into its range of the recorded global annual deposition fluxes, i.e., from 23 to 367 Bq m^{-2}. Zhang et al. (2021) developed empirical equations for calculating ^{210}Pb annual depositional fluxes using MAP. Using the equation for 30–40° N (^{210}Pb annual depositional fluxes = 0.13 MAP + 71.8; r = 0.39; p = 2.1 × 10^{-5}; n = 113), the value for our study site is 189 Bq m^{-2} yr^{-1}, which is quite consistent with our value.

No data has yet been published on $^{239+240}Pu$ inventories in Iran. The estimated reference inventory of 135 ± 31 Bq m^{-2} is considerably greater than the average value suggested for the global fallout of Pu in the 30 to 40°N latitude, at 42 Bq m^{-2} (UNSCEAR, 2000). this deviation from the global average value might be attributed to high initial bomb-derived depositions in the study site from 1953 to 1964. Table 4 summarizes $^{239+240}Pu$ inventories at reference sites around the globe. Our baseline inventory fell into the reported range by Guan et al. (2021), varying from 116.57 to 554 Bq m^{-2}, measured in areas with the same latitudes and similar MAPs in China (Table 5).

4.1.2. Fallout radionuclides inventories and soil redistribution rates at slope transects

The net soil erosion rates estimated by DMM at the forested hillslope were around 2 and 5.1 Mg ha^{-1} yr^{-1} for ^{137}Cs and $^{210}Pb_{ex}$, respectively. Different values were reported for the net soil erosion rates at forested areas in the literature (e.g. Wakiyama et al., 2010; Gaspar et al., 2013; Teramage et al., 2015; Meusburger et al., 2016; Gharibreza et al., 2013,

Table 4
Summary of soil physicochemical properties of the surface and subsurface soils at the forested and orchard hillslope (the statistical comparison was made between topsoil (0–20 cm) and subsoil (20–40 cm) properties of two land-uses separately). H-values of Kruskal–Wallis are also given for significant properties. (ECe: Electrical Conductivity, OM: Total Organic Matter, TN: Total Nitrogen, CCE: Carbonate Calcium Equivalent, CEC: Cation Exchange Capacity, BD: Bulk Density, *f*: Porosity, FC: soil water retention at potential equivalent to Field Capacity, PWP: Permanent Wilting Point, AWC: Available Water Content, PS: Percolation Stability, SI: Sealing Index, CI: Crusting Index, and K: soil erodibility).

Parameter	Topsoil			Subsoil		
	Forest	Vineyard	H-value	Forest	Vineyard	H-value
Clay (%)	21.0 ± 3.5[a†]	26.3 ± 5.8[a]		31.4 ± 1.6[A‡]	23.4 ± 2.7[B]	0.50
Silt (%)	54.0 ± 4.0[a]	50.3 ± 4.3[a]		51.1 ± 7.4[A]	53.2 ± 3.8[A]	
Sand (%)	25.0 ± 4.1[a]	23.4 ± 1.9[a]		17.5 ± 5.8[A]	23.4 ± 1.1[A]	
Gravel (%)	18.3 ± 6.7[a]	13.8 ± 5.5[a]		24.3 ± 9.3[A]	27.2 ± 7.0[A]	
pH	7.2 ± 0.2[b]	7.6 ± 0.3[a]	5.28	7.3 ± 0.1[B]	7.5 ± 0.2[A]	5.85
ECe (dS m^{-1})	2.0 ± 0.3[b]	2.40 ± 0.2[a]	6.27	1.6 ± 0.1[A]	1.45 ± 0.2[A]	
OM (%)	2.8 ± 0.3[a]	1.4 ± 0.3[b]	9.02	1.7 ± 0.1[A]	1.2 ± 0.2[B]	7.03
TN (gr kg^{-1})	0.20 ± 0.08[a]	0.16 ± 0.02[b]	0.43	0.16 ± 0.06[A]	0.12 ± 0.02[B]	0.78
C:N	72. 9 ± 20.3[a]	42.2 ± 4.1[b]	3.86	61.2 ± 22.2[A]	50.6 ± 12.7[A]	
CCE (%)	2.8 ± 0.9[a]	3.3 ± 0.3[a]		3.4 ± 0.3[A]	3. 8 ± 0.5[A]	
CEC ($cmol^{+}$ kg^{-1})	27.9 ± 0.8[a]	22.46 ± 0.9[b]	9.02	34.9 ± 1.6[A]	24.6 ± 0.2[B]	8.31
BD (Mg m^{-3})	1.1 ± 0.6[b]	1.4 ± 0.7[a]	9.02	1.3 ± 0.7[B]	1.6 ± 1.0[A]	8.34
f (%)	59.0 ± 2.1[a]	48.4 ± 2.8[b]	9.02	51.9 ± 2.7[A]	41.38 ± 3.6[B]	8.34
FC (%)	38.6 ± 1.3[a]	32.8 ± 1.6[b]	9.0	32.4 ± 1.1[A]	30.8 ± 1.2[B]	5.03
PWP (%)	15.6 ± 1.9[a]	14.9 ± 2.1[a]		14.4 ± 1.3[A]	14.4 ± 1.6[A]	
AWC (%)	23.0 ± 2.9[a]	17.9 ± 1.3[b]	7.37	18.0 ± 1.6[A]	16.4 ± 1.5[B]	8.31
PS (gr H_2O $600s^{-1}$)	309.4 ± 43.6[a]	137.9 ± 66.3[b]	9.44	160.4 ± 41.0[A]	101.2 ± 62.8[B]	1.19
SI (%)	3.84 ± 0.6[a]	1.9 ± 0.3[b]	8.16	2.2 ± 0.1[A]	1.5 ± 0.3[B]	7.0
CI	1.0 ± 0.1[b]	1.3 ± 0.1[a]	9.0	1.2 ± 0.1[B]	1.5 ± 0.1[A]	8.34
K (t ha hr MJ^{-1} ha^{-1} mm^{-1})	0.044 ± 0.005[b]	0.051 ± 0.009[a]	1.19	0.055 ± 0.005[B]	0.067 ± 0.005[A]	3.60

[†]Different lowercase letters indicate significant differences at the p-level<0.05 in topsoil properties of two land uses.
[‡]Different capital letters indicate significant differences at the p-level<0.05 in subsoil properties of two land uses.

2020). For instance, by using $^{210}Pb_{ex}$, Gaspar et al. (2013) estimated a mean soil redistribution rate of 1.3–1.7 Mg ha^{-1} yr^{-1} at the slope gradient of 24% in the Mediterranean oak forest, Spain. Wakiyama et al. (2010) reported soil erosion magnitudes obtained by $^{210}Pb_{ex}$ varying from 0.65 to 1.24 Mg ha^{-1} yr^{-1} in forested hillslopes with a slope gradient of around 40% in Japan. These values were, nonetheless, slightly lower than our estimated values.

The soil redistribution rates of three FRNs in a forested transect were estimated using both the MODERN model and DMM (Fig. 5b). Results obtained for ^{137}Cs by the MODERN represented a wider range of soil redistribution magnitude, while the DMM outputs tended to level off the extreme soil redistribution rates, which were in accordance with

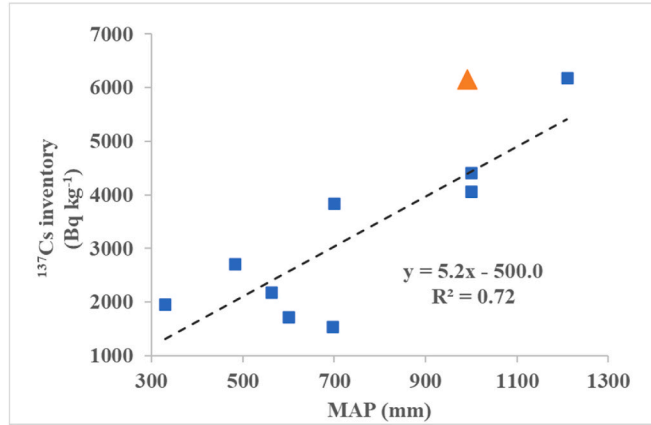

Fig. 7. The correlation between reported ^{137}Cs inventories and MAP in Iran (for more details, see Table 2). The orange triangle corresponds with our site. (For interpretation of the references to colour in this figure legend, the reader is referred to the Web version of this article.)

Table 5
$^{239+240}Pu$ baseline inventory and mean annual precipitation (MAP) in undisturbed locations.

Location	Mean Annual Precipitation (mm)	$^{239+240}Pu$ inventory at reference site (Bq m^{-2})	Reference
Australia	1200	8.8	Tims et al. (2013)
China	600–800	87 ± 3	Xu et al. (2013)
	800–1000	45 - 55 (in Hubei)	Zheng et al. (2009)
	235–238	32 (in Lanzhou)	Dong et al. (2010)
	500–1100	117–554 (in Qinghai-Tibet Plateau)	Guan et al. (2021)
South Korea	–	18 (in Sesan);	Lee et al. (1996)
	–	102 (in Euiwang)	Lee et al. (1996)
	1599	55 ± 8	Meusburger et al. (2016)
Europe	500–3500	8 - 380 (53.3)	Meusburger et al. (2020)
Germany	968	59 ± 8	Schimmack et al. (2001)
Switzerland	1400	67 ± 13 and 83 ± 11	Meusburger et al. (2018); Schaub et al. (2010); Alewell et al. (2014)
	1050	78 -104 (92)	Zollinger et al. (2015)
Congo	1300–1900	33-48 (41.3)	Wilken et al. (2021)

Meusburger et al. (2018).

At the vineyard hillslope, the net soil erosion rates estimated by MBM II were 25.9 ± 5.7 and 32.5 ± 14.5 Mg ha^{-1} yr^{-1} for ^{137}Cs and $^{210}Pb_{ex}$, respectively. Both FRNs estimated that soil erosion has increased by nearly five times following deforestation. Gharibreza et al. (2013), who used the ^{137}Cs method, showed that soil loss magnitude surged by 7–13 times following deforestation in a watershed in Malaysia, which was compatible with our findings.

It should be noted that different FRNs inherently account for diverse time spans (Meusburger et al., 2016). Relatively high ^{137}Cs Chernobyl input at the site under investigation (~50%) reveals that ^{137}Cs technique is more likely to indicate a medium-term soil erosion process, i.e., mainly from 1986 onwards. However, the time frame captured by $^{239+240}Pu$ has been recorded from the mid-1960s onward. Moreover, although $^{210}Pb_{ex}$ inventory reflects fallout depositions during the last 100 years, due to the radionuclide's ongoing fallout and a short half-life, it is more sensitive to the two last decades' erosive events causing soil redistribution (Porto et al., 2013, 2014). At the forested hillslope, the net soil erosion rate estimated by $^{239+240}Pu$ was far lower than that of ^{137}Cs

(Table 2), suggesting that a higher soil loss might have occurred after 1986 compared to the 1963–1986 time window. In both land-use types, the net soil erosion rates estimated by ^{137}Cs were slightly smaller than those of $^{210}Pb_{ex}$. Such an incongruity was also found in elsewhere, e.g. Japan (Wakiyama et al., 2010), China (Fang et al., 2013), and Iran (Khodadadi et al., 2018). The higher erosion rates may be interpreted as an accelerated trend in soil erosion, which could be a reflection of last decades' climate variabilities. A trend analysis of MAPs of two adjacent meteorological stations, Sanandaj and Marivan, was done using the Mann-Kendall test and Sen's slope estimates (Salmi et al., 2002). The MAPs of both stations showed a clear downward trend from 1959 onwards. Additionally, Balling et al. (2016) reported an increase in the number of extreme precipitation events in Iran from 1951 to 2007. This can suggest that erosion increased at the study site in response to climate variabilities over the last decades. However, as highlighted in similar studies, measurement uncertainties of $^{210}Pb_{ex}$ and related soil erosion rates are high. To illustrate, estimated net soil erosion uncertainty in the vineyard was about 10.8 Mg ha^{-1} yr^{-1}, almost twice as high as that of ^{137}Cs, and in the forest were 0.4 and 1.7 Mg ha^{-1} yr^{-1} for ^{137}Cs and $^{210}Pb_{ex}$, respectively. On the whole, changes in land use and land management (Gaspar et al., 2013; Zhang et al., 2006), microtopography, and rainfall characteristics in various timescales might have a significant effect on estimated soil erosion rates using different FRNs. Moreover, the soil redistribution patterns in both hillslopes were controlled mainly by topography (Fig. 6). Nevertheless, no significant correlations were found between slope gradient and curvature and soil redistribution rates estimated by both radionuclides at the p-level of 0.05, being in accordance with Fang et al.'s (2013) findings.

4.2. Assessment of soil physicochemical properties in the vineyard and forested hillslopes

Soil organic matter content (OM), a main indicator of soil quality and health (Gregorich et al., 2006), influences soil's chemical, physical, and biological properties, therefore directly impacting microbial and plant growth. In general, factors such as low vegetation cover, less shading, increased soil temperature, tillage operations, and soil erosion susceptibility following deforestation are key elements prompting the loss of OM (Six et al., 2000). OM and TN in both depths were significantly lower in the vineyard compared to the forest (Table 4). Puget and Lal (2005), Khormali et al. (2009), and Nabiollahi et al. (2018) also pointed out considerable reductions in SOM after land-use change, congruent with our findings, which can partly be due to a lower litter turnover and higher biomass exiting the hillslope, i.e. roughly around 8 Mg C ha^{-1} in the vineyard vs. 1 in the forest within 35 years. In addition, manual tillage practices in the vineyard that are done to eliminate weed growth and conserve moisture may increase OM oxidation by breaking up the soil aggregates (Nardi et al., 1996). Here, SOCS decreased by 29% in 0–40 cm depth following the conversion of forest to cropland. A range of values for SOCS decline following deforestation can be found in the literature, e.g. from 20% reported by Arias-Ortiz et al. (2021) in Madagascar and de Blécourt et al. (2019) in Namibia to significantly higher values, for example, Rojas et al. (2016) up to 45% and Conti et al. (2014) at 64% in Argentina, An et al. (2008) at 72% in China, and Assefa et al. (2017) at 70% in Ethiopia. Such diverse values can be attributed to differences between climate, initial SOCS, management practices, and soil type (Stevens and van Wesemael, 2008). Forest soils had a higher C:N ratio in both depths, which was comparable to those reported by Puget and Lal (2005). In fact, the ratio mostly corresponds to the amounts of plant residuals entering soil OM pool (Puget and Lal, 2005). As it is expected that the C:N ratio dropped with depth in both soils, most probably as a result of lower OM turnover (Table 4).

PSs in forest and vineyard topsoil were categorized as rapid and moderate, in respective order. Rapid PS in the forest indicates that soils are generally strongly structured, while moderate PS in vineyard soils implies low aggregate stability triggered by lower OM content. It is also believed that fungal hyphae play an essential role in aggregate stability in forests (Ternan et al., 1996). Mbagwu and Auerswald (1999) also reported rapid PS in forest soils and slow to moderate PS values in bare fallows and cultivated lands. They concluded that PS positively correlated with OM. Notable is that the PSs of topsoil samples in both land uses were higher than those of their subsoils. Moreover, the PS of the topsoil in the vineyard site was roughly as the same as that of the subsoil of the forest, implying the possibility of the vineyard's topsoil removal by erosion. Among all properties shown in Table 4, the highest coefficient of variability occurred in PS.

Microaggregates resulting from aggregate breakdown can clog large pores, thus decreasing infiltration rate and increasing runoff generation (Auerswald, 1995). SI in all soil samples was less than 5%, indicating a high risk of sealing due to a high percentage of silt (Valentin and Bresson, 1997). However, SI was significantly higher in both depth intervals of the forest owing to higher OM content. Udom and Kamalu (2016) reported that SI varied from 2.40 to 3.10 in topsoil and from 2.17 to 4.76 in the subsoil of tropical soils susceptible to seasonal flooding, meaning that the risk of sealing was considerably high in their investigated sites. In contrast, CI in both the topsoil and subsoil of the forest showed a low sealing risk, while it was considered to have a moderate sealing risk in the surface and subsurface soils of the vineyard. In other words, although SI indicated a high risk of sealing for all studied soils, CI suggested that crusting risks in both surface and subsurface soils of the vineyard were more than those of forest soils. This implies that CI can be an advantageous index over SI as it can not only take the particle size classes of silt (i.e., fine and coarse silt) into consideration but also better differentiate between the soils with different OM.

The K factor depends on PSD, permeability, OM content, and structure. K-values in forest surface and subsurface soils were lower than those for vineyard soils. The reported K factor in China, ranging from 0.007 to 0.043 t ha hr MJ^{-1} ha^{-1} mm^{-1} (Wang et al., 2013), and the values observed in the USA, varying from 0.004 to 0.063 t ha hr MJ^{-1} ha^{-1} mm^{-1} (Wischmeier and Smith, 1978), indicate that soil erodibility in the study area was relatively high. In other words, the soils of both land uses are extremely prone to soil erosion owing to high amounts of silt. Following the land-use change, the K factor value in the vineyard increased to 14% in topsoil and around 20% in the subsoil, which was in agreement with Khormali et al. (2009),. Referring to the study of Sanchez-Maranon et al. (2002), following the land-use change, the K-value rose to around 59% in southern Spain. Also, Celik (2005) studied the impact of cultivated land on soil properties in the south of Turkey and reported that cultivation practices had increased the amount of K-value by 2.4.

The most sensitive physicochemical properties to deforestation were indicated by the H-values of the Kruskal–Wallis test (Table 4). For the surface soils of two land-use types, the highest H-values were detected to be PS at 9.44, followed closely by OM, CEC, BD, *f*, FC, and CI ($9.0 <$ H-value <9.20). In contrast, the highest H-values for subsurface soils were CEC, BD, *f*, AWC, and CI ($8.31 <$ H-value <8.34) (Table 4). PS in subsurface soils was, therefore, not an appropriate metric to discriminate between subsoils, while being a reliable property in topsoils.

In brief, vineyard topsoil experienced the most dramatic drops in PS, SI, and OM at about 55, 51, and 49%, respectively, while AWC, TN, CEC, and porosity witnessed a lower decline, ranging between 18 and 22%. In contrast, soil loss estimated by ^{137}Cs, CI, EC, soil loss estimated by $^{210}Pb_{ex}$, and BD rose considerably, between 18 and 22% (Fig. 8a). In the subsurface layer, similar to topsoil, PS, OM, and SI declined by 37, 32, and 30%, respectively, but unlike topsoil, CEC and clay content exhibited a 29 and 25% decrease. On the other hand, BD, K, and CI soared by 21, 22, and 32%, in turn (Fig. 8b). Strikingly, most forest subsoil properties were quite comparable with vineyard topsoil rather than vineyard subsoil. To illustrate, the average values of BD, *f*, FC, and AWC and, to some extent, PS, SI, CI, K, and OM in vineyard's topsoil and forest's subsoil were remarkably similar (Table 4). For one thing, the depth of soil loss in the vineyard is estimated to be roughly around 10 cm

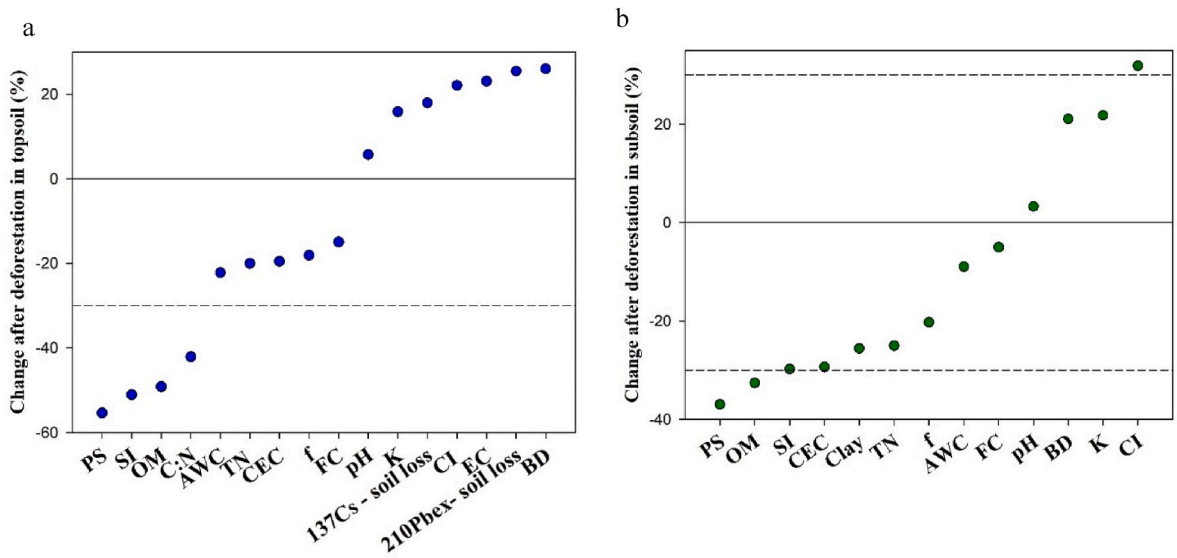

Fig. 8. Percentage of change in soil physicochemical properties in topsoil (0–20 cm; a) and subsoil (20–40 cm; b) in the vineyard and forested hillslopes (mean of the properties with a significant difference in forested and vineyard sites were used; see Table 5).

utilizing ^{137}Cs-derived net erosion. Moreover, the soil was continuously mixed with subsoil underneath by tillage operations (ca. upper 20 cm), which may result in the vineyard's topsoil showing relatively similar behavior to forest subsoil, findings being in agreement with An et al. (2008). Noteworthy is that the deterioration of soil's physical properties, e.g. PS, BD, and *f* was incredibly high after deforestation, which was in line with Tobón et al.'s (2010) findings. Overall, these alterations in surface and sub-surface soil properties verified a deterioration of soil quality within 35 years post deforestation.

5. Conclusion

Over the past decades, a rapidly growing population has increased the demand for food, leading to rapid land-use changes in the country, i.e., conversion of land under natural vegetation into arable lands. The present study was conducted to quantify the impacts of deforestation on soil loss using different fallout radionuclides and soil physicochemical properties.

The proportion of ^{137}Cs fallout from different sources (Chernobyl fallout vs. global fallout) could be determined via $^{239+240}$Pu isotopes. The ^{240}Pu/^{239}Pu atom ratios confirmed that Pu originated exclusively from global fallout. From the ^{137}Cs/$^{239+240}$Pu ratio, it was evident that around half of the ^{137}Cs found at the site was Chernobyl-derived. $^{239+240}$Pu proved to be a reliable tool to quantify the relative contribution of Chernobyl-derived ^{137}Cs in contaminated areas, a prerequisite necessary to applying ^{137}Cs conversion models. Both ^{137}Cs and ^{210}Pb$_{ex}$ radionuclides indicated that deforestation increased annual soil loss by about five times. Notable is that the values obtained by both techniques for each land use were consistent; however, moderately higher net soil erosion rates were estimated by ^{210}Pb$_{ex}$ at both sites.

The conversion of forest to vineyard led to marked deterioration in soil quality as was highlighted by a significant decrease in OM, TN, C:N, CEC, AWC, *f*, and PS, and a substantial increase in ECe, pH, BD, and K factor in both topsoil and subsoil. SOCS in 0–40 cm depth dropped by 14 Mg C ha^{-1}, from 49 Mg C ha^{-1} in the forest to 35 Mg C ha^{-1} in the vineyard. As such, about 8 Mg C ha^{-1} in the vineyard was removed by erosion within 35 years, and the remaining 6 Mg C ha^{-1} seemed to be lost via CO_2 emissions. This net atmospheric carbon emissions, at 17.1 kg C m^{-2} yr^{-1}, was in accordance with values reported by Dialynas et al. (2016) at 18.2 kg C m^{-2} yr^{-1} and Harden et al. (1999) at 10–20 kg C m^{-2} yr^{-1}. This signifies the impacts of accelerated soil erosion on SOC terrestrial storage (Ito, 2007), including SOC redistribution within agricultural landscapes and carbon oxidation (McCarty and Ritchie, 2002). Thus, carbon erosion and deposition may exert strong controls over the land's potential to act as a carbon source or a sink (Dialynas et al., 2016). Indeed, land-use change can be considered to be one of the main causes of carbon emissions, contributing to climate change (Watson et al., 2000).

Despite the relatively higher slope gradient and length of the forested hillslope, the surface soils of the vineyard were more susceptible to aggregate breakdown, sealing, compaction, drought, and erosion while undergoing intensive soil, SOC, and nutrient loss processes. Not only that, but the decline in soil quality also reached the subsoil. Taking all these into account, these high amounts of net soil erosion in the vineyard can give rise to off-site impacts of soil erosion, including downstream sediment deposition in fields, floodplains, and water bodies, where suspended sediments reduce water quality (Verstraeten and Poesen, 2000). The situation is expected to worsen under future climate change conditions, so much so that rills and gullies will be formed as a result of erosion. Among all measured physicochemical properties, PS had the highest H-value of the Kruskal–Wallis test (9.44), thus considered to be the most sensitive element to land-use change. More precisely, PS was proven to be a powerful tool for studying soil aggregate stability and quality, being cost-effective and less labor intense. Overall converting forests to vineyards caused soil quality to deteriorate, which will likely impact soil productivity and food security and, more importantly, affect the water quality of the lake and greenhouse gas emissions.

Author contribution

Maral Khodadadi: Funding acquisition, Investigation, Resources, Data curation, Software, Writing- Original draft preparation. **Christine Alewell:** Supervision, Writing - Review & Editing. **Mohammad Mirzaei:** Investigation. **Ehssan Ehssan-Malahat:** Investigation. **Farrokh Asadzadeh:** Investigation. **Peter Strauss:** Investigation. **Katrin Meusburger:** Conceptualization, Methodology, Software, Validation, Writing - Review & Editing.

Declaration of competing interest

The authors declare that they have no known competing financial interests or personal relationships that could have appeared to influence the work reported in this paper.

Data availability

The authors do not have permission to share data.

Acknowledgments

This study has been finalized to support the IAEA Coordinated Research Project (CRP) on "*Nuclear techniques for a better understanding of the impact of climate change on soil erosion in upland agro-ecosystems*" (D1.50.17).

References

Afshar, F.A., Ayoubi, S., Jalalian, A., 2010. Soil redistribution rate and its relationship with soil organic carbon and total nitrogen using ^{137}Cs technique in a cultivated complex hillslope in western Iran. J. Environ. Radioact. 101 (8), 606–614. https://doi.org/10.1016/j.jenvrad.2010.03.008.

Alewell, C., Meusburger, K., Juretzko, G., Mabit, L., Ketterer, M.E., 2014. Suitability of $^{239+240}$Pu and ^{137}Cs as tracers for soil erosion assessment in mountain grasslands. Chemosphere 103, 274–280. https://doi.org/10.1016/j.chemosphere.2013.12.016.

Alewell, C., Pitois, A., Meusburger, K., Ketterer, M., Mabit, L., 2017. 239+240Pu from "contaminant" to soil erosion tracer: where do we stand? Earth Sci. Rev. 172, 107–123. https://doi.org/10.1016/j.earscirev.2017.07.009.

An, S., Zheng, F., Zhang, F., Van Pelt, S., Hamer, U., Makeschin, F., 2008. Soil quality degradation processes along a deforestation chronosequence in the Ziwuling area, China. Catena 75 (3), 248–256.

Arata, L., Alewell, C., Frenkel, E., A'Campo-Neuen, A., Iurian, A.R., Ketterer, M.E., Mabit, L., Alewell, C., 2016a. Modelling Deposition and Erosion rates with RadioNuclides (MODERN)-Part 2: a comparison of different models to convert $^{239+240}$Pu inventories into soil redistribution rates at unploughed sites. J. Environ. Radioact. 162, 97–106. https://doi.org/10.1016/j.jenvrad.2016.05.009.

Arata, L., Meusburger, K., Frenkel, E., A'Campo-Neuen, A., Iurian, A.R., Ketterer, M.E., Mabit, L., Meusburger, K., 2016b. Modelling Deposition and Erosion rates with RadioNuclides (MODERN)-Part 1: a new conversion model to derive soil redistribution rates from inventories of fallout radionuclides. J. Environ. Radioact. 162, 45–55. https://doi.org/10.1016/j.jenvrad.2016.05.008.

Arias-Ortiz, A., Masqué, P., Glass, L., Benson, L., Kennedy, H., Duarte, C.M., Garcia-Orellana, J., Benitez-Nelson, C.R., Humphries, M.S., Ratefinjanahary, I., Ravelonjatovo, J., 2021. Losses of soil organic carbon with deforestation in mangroves of Madagascar. Ecosystems 24 (1), 1–19. https://doi.org/10.1007/s10021-020-00500-z.

Assefa, D., Rewald, B., Sandén, H., Rosinger, C., Abiyu, A., Yitaferu, B., Godbold, D.L., 2017. Deforestation and land use strongly effect soil organic carbon and nitrogen stock in Northwest Ethiopia. Catena 153, 89–99. https://doi.org/10.1016/j.catena.2017.02.003.

Auerswald, K., 1995. Percolation stability of aggregates from arable topsoils. Soil Sci. 159 (2), 142.

Balling, R.C., Keikhosravi Kiany, M.S., Sen Roy, S., Khoshhal, J., 2016. Trends in extreme precipitation indices in Iran: 1951-2007. Adv. Meteorol. https://doi.org/10.1155/2016/2456809, 2016.

Berthon, V., Bouchez, A., Rimet, F., 2011. Using diatom life-forms and ecological guilds to assess organic pollution and trophic level in rivers: a case study of rivers in south-eastern France. Hydrobiologia 673, 259–271. https://doi.org/10.1007/s10750-011-0786-1.

Blake, G.R., Hartge, K.H., 1986. Methods of soil analysis. In: Klute, A. (Ed.), Part 1: Physical and Mineralogical Methods, second ed. ASA, Madison, WI, A.

Bremner, J.M., 1996. Nitrogen-total. In: Bigham, F.T. (Ed.), Methods of Soil Analyses, Part III, Chemical Methods. SSSA, Madison, WI, pp. 1085–1184.

Campbell, B.L., Loughran, R.J., Elliott, G.L., 1988. A Method for Determining Sediment Budgets Using Caesium-137, Sediment Budgets. IAHS Publication, 174.

Celik, I., 2005. Land-use effects on organic matter and physical properties of soil in a southern Mediterranean highland of Turkey. Soil Tillage Res. 83 (2), 270–277. https://doi.org/10.1016/j.still.2004.08.001.

Conti, G., Pérez-Harguindeguy, N., Quètier, F., Gorné, L.D., Jaureguiberry, P., Bertone, G.A., Enrico, L., Cuchietti, A., Díaz, S., 2014. Large Changes in Carbon Storage under Different Land-Use Regimes in Subtropical Seasonally Dry Forests of Southern South America, vol. 197. Agriculture, ecosystems & environment, pp. 68–76. https://doi.org/10.1016/j.agee.2014.07.025.

Danielson, R.E., Sutherland, P.L., 1986. Porosity. In: Klute, A. (Ed.), Methods of Soil Analysis: Part 1 Physical and Mineralogical Methods, vol. 5, pp. 443–461.

de Blécourt, M., Gröngröft, A., Baumann, S., Eschenbach, A., 2019. Losses in soil organic carbon stocks and soil fertility due to deforestation for low-input agriculture in semi-arid southern Africa. J. Arid Environ. 165, 88–96. https://doi.org/10.1016/j.jaridenv.2019.02.006.

DEI, Department of environment Iran, 2003. Initial National Communication to UNFCCC.

Dialynas, Y.G., Bastola, S., Bras, R.L., Billings, S.A., Markewitz, D., Richter, D.D., 2016. Topographic variability and the influence of soil erosion on the carbon cycle. Global Biogeochem. Cycles 30 (5), 644–660. https://doi.org/10.1002/2015GB005302.

Dong, W., Tims, S.G., Fifield, L.K., Guo, Q., 2010. Concentration and characterization of plutonium in soils of Hubei in central China. J. Environ. Radioact. 101 (1), 29–32. https://doi.org/10.1016/j.jenvrad.2009.08.011.

Emadodin, I., Narita, D., Bork, H.R., 2012. Soil degradation and agricultural sustainability: an overview from Iran. Environ. Dev. Sustain. 14 (5), 611–625. https://doi.org/10.1007/s10668-012-9351-y.

Fageria, N.K., Baligar, V.C., Jones, C.A., 2010. Growth and Mineral Nutrition of Field Crops. CRC Press.

Fang, H.Y., Sheng, M., Tang, Z.H., Cai, Q.G., 2013. Assessment of soil redistribution and spatial pattern for a small catchment in the black soil region, Northeastern China: using fallout ^{210}Pb$_{ex}$. Soil Tillage Res. 133, 85–92.

FAO, 1978. A Provisional Methodology for Soil Degradation Assessment, p. 84. Rome, Italy.

Foucher, A., Chaboche, P.-A., Sabatier, P., Evrard, O., 2021. A worldwide meta-analysis (1977-2020) of sediment core dating using fallout radionuclides including ^{137}Cs and ^{210}Pb$_{xs}$. Earth Syst. Sci. Data 13, 4951–4966. https://doi.org/10.5194/essd-13-4951-2021.

Garcia Agudo, E., 1998. Global Distribution of {sup 137} Cs Inputs for Soil Erosion and Sedimentation Studies.

Gaspar, L., Navas, A., Machín, J., Walling, D.E., 2013. Using ^{210}Pb$_{ex}$ measurements to quantify soil redistribution along two complex toposequences in Mediterranean agroecosystems, northern Spain. Soil Tillage Res. 130, 81–90. https://doi.org/10.1016/j.still.2013.02.011.

Gee, G.W., Bauder, J.W., 1986. Particle-size analysis, 2nd edn., Agronomy, 9. In: Klute, A. (Ed.), Methods of Soil Analysis: Part 1. Physical and Mineralogical Methods. Soil Science Society of America, Madison, USA, pp. 383–411.

Gharibreza, M., Raj, J.K., Yusoff, I., Othman, Z., Tahir, W.Z.W.M., Ashraf, M.A., 2013. Land use changes and soil redistribution estimation using ^{137}Cs in the tropical Bera Lake catchment, Malaysia. Soil Tillage Res. 131, 1–10. https://doi.org/10.1016/j.still.2013.02.010.

Gharibreza, M., Zaman, M., Porto, P., Fulajtar, E., Parsaei, L., Eisaei, H., 2020. Assessment of deforestation impact on soil erosion in loess formation using ^{137}Cs method (case study: golestan Province, Iran). Int. Soil Water Cones. https://doi.org/10.1016/j.iswcr.2020.07.006.

Gharibreza, M., Samani, A.B., Arabkhedri, M., Zaman, M., Porto, P., Kamali, K., Sobh-Zahedi, S., 2021. Investigation of on-site implications of tea plantations on soil erosion in Iran using ^{137}Cs method and RUSLE. Environ. Earth Sci. 80 (1), 1–14. https://doi.org/10.1007/s12665-020-09347-y.

Gregorich, E.G., Beare, M.H., McKim, U.F., Skjemstad, J.O., 2006. Chemical and biological characteristics of physically uncomplexed organic matter. Soil Sci. Soc. Am. J. 70 (3), 975–985. https://doi.org/10.2136/sssaj2005.0116.

Guan, Y., Zhang, P., Huang, C., Wang, D., Wang, X., Li, L., Han, X., Liu, Z., 2021. Vertical distribution of Pu in forest soil in Qinghai-Tibet Plateau. J. Environ. Radioact. 229, 106548.

Harden, J.W., Sharpe, J.M., Parton, W.J., Ojima, D.S., Fries, T.L., Huntington, T.G., Dabney, S.M., 1999. Dynamic replacement and loss of soil carbon on eroding cropland. Global Biogeochem. Cycles 13 (4), 885–901.

Hiederer, R., Köchy, M., 2011. Global soil organic carbon estimates and the harmonized world soil database. EUR 79, 25225.

Hodge, V., Smith, C., Whiting, J., 1996. Radiocesium and plutonium: still together in "background" soils after more than thirty years. Chemosphere 32, 2067–2075. https://doi.org/10.1016/0045-6535(96)00108-7.

IAEA, 2014. Guidelines for Using Fallout Radionuclides to Assess Erosion and Effectiveness of Soil Conservation Strategies. IAEA TECDOC No. 1741, p. 215.

Ito, A., 2007. Simulated impacts of climate and land-cover change on soil erosion and implication for the carbon cycle, 1901 to 2100. Geophys. Res. Lett. 34 (9) https://doi.org/10.1029/2007GL029342.

Jackson, M.L., 1958. Soil Chemical Analysis, vol. 498. prentice Hall. Inc., Englewood Cliffs, NJ, pp. 183–204.

Kalhor, M., 1998. Comparison of Cs-137 and USLE Methods to Estimate the Soil Loss of Rimeleh Watershed (Lorestan Province), MSc Thesis in Soil Science. College of Agriculture, Isfahan University of Technology, Isfahan (In Persian).

Karger, D.N., Conrad, O., Böhner, J., Kawohl, T., Kreft, H., Soria-Auza, R.W., Kessler, M., 2017. Climatologies at high resolution for the earth's land surface areas. Sci. Data 4, 20. https://doi.org/10.1038/sdata.2017.122.

Ketterer, M.E., Szechenyi, S.C., 2008. Determination of plutonium and other transuranic elements by inductively coupled plasma mass spectrometry: a historical perspective and new frontiers in the environmental sciences. Spectrochim. Acta B Atom Spectrosc. 63 (7), 719–737. https://doi.org/10.1016/j.sab.2008.04.018.

Kelley, J.M., Bond, L.A., Beasley, T.M., 1999. Global distribution of Pu isotopes and ^{237}Np. Sci. Total Environ. 483–500. https://doi.org/10.1016/S0048-9697(99)00160-6.

Ketterer, M.E., Hafer, K.M., Mietelski, J.W., 2004. Resolving Chernobyl vs. global fallout contributions in soils from Poland using Plutonium atom ratios measured by inductively coupled plasma mass spectrometry. J. Environ. Radioact. 73 (2), 183–201. https://doi.org/10.1016/j.jenvrad.2003.09.001.

Ketterer, M.E., Zheng, J., Yamada, M., 2012. Applications of transuranics as tracers and chronometers in the environment. In: Handbook of Environmental Isotope Geochemistry. Springer, Berlin, Heidelberg, pp. 395–417.

Khodadadi, M., Mabit, L., Zaman, M., Paolo, P., Gorji, M., 2018. Evaluating the efficiency of soil conservation measures on erosion rates using ^{137}Cs and ^{210}Pb$_{ex}$ methods for semi-arid farm lands: a case study in the Kouhin region of Qazvin Province in Iran. J. Soils Sediments. https://doi.org/10.1007/s11368-018-2205-y.

Khormali, F., Ajami, A., Ayoubi, S., Srinivasarao, C.H., Wani, S.P., 2009. Role of deforestation and hillslope position on soil quality attributes of loess-derived soils in Golestan province, Iran. Agric. Ecosyst. Environ. 134, 178–189. https://doi.org/10.1016/j.agee.2009.06.017.

Klute, A., 1986. Water retention: laboratory methods. In: Klute, A. (Ed.), Methods of Soil Analysis: Part 1. Physical and Mineralogical Methods, pp. 635–662. ASA Monograph Number 9.

Lal, R., Tims, S.G., Fifield, L.K., Wasson, R.J., Howe, D., 2013. Applicability of ^{239}Pu as a tracer for soil erosion in the wet-dry tropics of northern Australia. Nucl. Instrum. Methods B 294, 577–583. https://doi.org/10.1016/j.nimb.2012.07.041.

Lee, M., Lee, C., Hong, K., Choi, Y., Boo, B., 1996. Depth distribution of $^{239,\ 240}$Pu and ^{137}Cs in soils of South Korea. J. Radioanal. Nucl. Chem. 204 (1), 135–144. https://doi.org/10.1007/BF02060874.

Mabit, L., Bernard, C., 2007. Assessment of spatial distribution of fallout radionuclides through geostatistics concept. J. Environ. Radioact. 97 (2–3), 206–219. https://doi.org/10.1016/j.jenvrad.2007.05.008.

Mabit, L., Benmansour, M., Walling, D.E., 2008. Comparative advantages and limitations of the fallout radionuclides ^{137}Cs, ^{210}Pb$_{ex}$ and ^{7}Be for assessing soil erosion and sedimentation. J. Environ. Radioact. 99 (12), 1799–1807. https://doi.org/10.1016/j.jenvrad.2008.08.009.

Mabit, L., Klik, A., Benmansour, M., Toloza, A., Geisler, A., Gerstmann, U.C., 2009. Assessment of erosion and deposition rates within an Austrian agricultural watershed by combining ^{137}Cs, ^{210}Pb$_{ex}$ and conventional measurements. Geoderma 150 (3–4), 231–239.

Mabit, L., Chhem-Kieth, S., Toloza, A., Vanwalleghem, T., Bernard, C., Amate, J.I., de Molina, M.G., Gómez, J.A., 2012. Radioisotopic and physicochemical background indicators to assess soil degradation affecting olive orchards in southern Spain. Agric. Ecosyst. Environ. 159, 70–80. https://doi.org/10.1016/j.agee.2012.06.014.

Matinfar, H., Kalhor, M., Shabani, A., Arkhi, S., 2013. Estimating soil erosion and sedimentation using Cesium-137 method: a case study (Raymaleh watershed, Lorestan). J. Agri. Eng. 35 (2), 37–54 (In Persian).

Mbagwu, J.S.C., Auerswald, K., 1999. Relationship of percolation stability of soil aggregates to land use, selected properties, structural indices and simulated rainfall erosion. Soil Tillage Res. 50 (3–4), 197–206. https://doi.org/10.1016/S0167-1987(99)00006-9.

McCarty, G.W., Ritchie, J.C., 2002. Impact of soil movement on carbon sequestration in agricultural ecosystems. Environ. Pollut. 116 (3), 423–430. https://doi.org/10.1016/S0269-7491(01)00219-6.

McLean, E.O., Oloya, T.O., Mostaghimi, S., 1982. Improved corrective fertilizer recommendations based on a two-step alternative usage of soil tests: I. Recovery of soil-equilibrated phosphorus. Soil Sci. Soc. Am. J. 46 (6), 1193–1197. https://doi.org/10.2136/sssaj1982.03615995004600060015x.

Meusburger, K., Mabit, L., Park, J.H., Sandor, T., Porto, P., Alewell, C., 2016. A multi-radionuclide approach to evaluate the suitability of $^{239+240}$Pu as soil erosion tracer. Sci. Total Environ. 566–567, 1489–1499. https://doi.org/10.1016/j.scitotenv.2016.06.035.

Meusburger, K., Porto, P., Mabit, L., La Spada, C., Arata, L., Alewell, C., 2018. Excess Lead-210 and Plutonium-239+240: two suitable radiogenic soil erosion tracers for mountain grassland sites. Environ. Res. 160, 195–202. https://doi.org/10.1016/j.envres.2017.09.02.

Meusburger, K., Evrard, O., Alewell, C., Borrelli, P., Cinelli, G., Ketterer, M., Mabit, L., Panagos, P., Van Oost, K., Ballabio, C., 2020. Plutonium aided reconstruction of caesium atmospheric fallout in European topsoils. Sci. Rep. 10 (1), 1–16. https://doi.org/10.1038/s41598-020-68736-22020.

Mietelski, J.W., Was, B., 1995. Plutonium from Chernobyl in Poland. Appl. Radiat. Isot. 46 (11), 1203–1211. https://doi.org/10.1016/0969-8043(95)00162-7.

Muramatsu, Y., Rühm, W., Yoshida, S., Tagami, K., Uchida, S., Wirth, E., 2000. Concentrations of ^{239}Pu and ^{240}Pu and their isotopic ratios determined by ICP-MS in soils collected from the Chernobyl 30-km zone. Environ. Sci. Technol. 34 (14), 2913–2917. https://doi.org/10.1021/es0008968.

Nabiollahi, K., Golmohamadi, F., Taghizadeh-Mehrjardi, R., Kerry, R., Davari, M., 2018. Assessing the effects of slope gradient and land use change on soil quality degradation through digital mapping of soil quality indices and soil loss rate. Geoderma 318, 16–28. https://doi.org/10.1016/j.geoderma.2017.12.024.

Nardi, S., Cocheri, G., Dell'Agnola, G., 1996. Biological activity of humus. In: Humic Substances in Terrestrial Ecosystems. Piccolo. A. Elsevier, Amsterdam, pp. 361–406.

Nelson, D.W., Sommers, L.E., 1982. Total carbon, organic carbon and organic matter. In: Page, A.L. (Ed.), Methods of Soil Analysis: Part 2. Chemical and Microbiological Properties, ASA Monograph Number 9, pp. 539–579.

Nunes, A.N., De Almeida, A.C., Coelho, C.O., 2011. Impacts of land use and cover type on runoff and soil erosion in a marginal area of Portugal. Appl. Geogr. 31 (2), 687–699. https://doi.org/10.1016/j.apgeog.2010.12.006.

Oliver, M.A., Webster, R., 2015. Basic Steps in Geostatistics: the Variogram and Kriging. Springer International Publishing, Cham, pp. 15–42.

Porto, P., Walling, D.E., Callegari, G., 2013. Using ^{137}Cs and ^{210}Pb$_{ex}$ measurements to investigate the sediment budget of a small forested catchment in southern Italy. Hydrol. Process. 27 (6), 795–806. https://doi.org/10.1002/hyp.9471.

Porto, P., Walling, D.E., Capra, A., 2014. Using ^{137}Cs and ^{210}Pb$_{ex}$ measurements and conventional surveys to investigate the relative contributions of interrill/rill and gully erosion to soil loss from a small cultivated catchment in Sicily. Soil Tillage Res. 135, 18–27. https://doi.org/10.1016/j.still.2013.08.013.

Puget, P., Lal, R., 2005. Soil organic carbon and nitrogen in a Mollisol in central Ohio as affected by tillage and land use. Soil Till. Res. 80, 201–213. https://doi.org/10.1016/j.still.2004.03.018.

Rhoades, J.D., 1982. Soluble salts. In: Page, A.L. (Ed.), Methods of Soil Analysis: Part 2: Chemical and Microbiological Properties. Monograph Number 9, second ed. ASA, Madison, WI, pp. 167–179.

Rojas, J.M., Prause, J., Sanzano, G.A., Arce, O.E.A., Sánchez, M.C., 2016. Soil quality indicators selection by mixed models and multivariate techniques in deforested areas for agricultural use in NW of Chaco, Argentina. Soil Tillage Res. 155, 250–262. https://doi.org/10.1016/j.still.2015.08.010.

Salmi, T., Määttä, A., Anttila, P., Ruoho-Airola, T., Amnell, T., 2002. Detecting trends of annual values of atmospheric pollutants by the Mann-Kendall test and Sen's slope estimates-The excel template application Makesens. Publ. Air Qual. 31.

Sanchez-Maranon, M., Soriano, M., Delgado, G., Delgado, R., 2002. Soil quality in Mediterranean mountain environments: effects of land use change. Soil Sci. Soc. Am. J. 66 (3), 948–958. https://doi.org/10.2136/sssaj2002.0948.

Schaub, M., Konz, N., Meusburger, K., Alewell, C., 2010. Application of in-situ measurement to determine ^{137}Cs in the Swiss Alps. J. Environ. Radioact. 101 (5), 369–376. https://doi.org/10.1016/j.jenvrad.2010.02.005.

Schimmack, W., Auerswald, K., Bunzl, K., 2001. Can $^{239+}$ ^{240}Pu replace ^{137}Cs as an erosion tracer in agricultural landscapes contaminated with Chernobyl fallout? J. Environ. Radioact. 53 (1), 41–57. https://doi.org/10.1016/S0265-931X(00)00117-X.

Scholten, T., 1997. Hydrology and erodibility of the soils and saprolite cover of the Swaziland Middleveld. Soil Technol. 11 (3), 247–262. https://doi.org/10.1016/S0933-3630(97)00011-1.

Seyedalipour, H., Feiznia, S., Ahmadi, H., Zare, M.R., Hosseinalizadeh, M., 2014. Comaprison of soil erosion by ^{137}CS and RUSLE-3D for loess deposits north-east of Iran (study area: aghemam catchment). J. Water. Soil. Cons. 21 (5), 27–47 (In Persian).

Shahoei, S., Rafahi, H., 1998. Assessment the impacts of erosion on soil properties and productivity of cropland in a part of Gorgan Watershed. Iran. J. Agric. Sci. 29, 1–18 (In Persian).

Siegrist, S., Schaub, D., Pfiffner, L., Mäder, P., 1998. Does organic agriculture reduce soil erodibility? The results of a long-term field study on loess in Switzerland. Agric. Ecosyst. Environ. 69 (3), 253–264. https://doi.org/10.1016/S0167-8809(98)00113-3.

Six, J., Paustian, K., Elliott, E.T., Combrink, C., 2000. Soil structure and organic matter I. Distribution of aggregate-size classes and aggregate-associated carbon. Soil Sci. Soc. Am. J. 64 (2), 681–689. https://doi.org/10.2136/sssaj2000.642681x.

Stevens, A., van Wesemael, B., 2008. Soil organic carbon stock in the Belgian Ardennes as affected by afforestation and deforestation from 1868 to 2005. For. Ecol. Manag. 256 (8), 1527–1539. https://doi.org/10.1016/j.foreco.2008.06.041.

Taxonomy, Soil, 2014. Soil Survey Staff. Keys to Soil Taxonomy, tenth ed. United States Department of Agriculture, Natural Resources Conservation Services, p. 331.

Teramage, M.T., Onda, Y., Wakiyama, Y., Kato, H., Kanda, T., Tamura, K., 2015. Atmospheric ^{210}Pb as a tracer for soil organic carbon transport in a coniferous forest. Environ. Sci. J. Integr. Environ. Res.: Process. Impacts 17 (1), 110–119.

Ternan, J.L., Elmes, A., Williams, A.G., Hartley, R., 1996. Aggregate stability of soils in central Spain and the role of land management. Earth Surf. Process. Landforms 21 (2), 181–193. https://doi.org/10.1002/(SICI)1096-9837(199602)21:2<181::AID-ESP622>3.0.CO;2-7.

Tims, S.G., Fifield, L.K., Hancock, G.J., Lal, R.R., Hoo, W.T., 2013. Plutonium isotope measurements from across continental Australia. Nucl. Instrum. Methods Phys. Res. Sect. B Beam Interact. Mater. Atoms 294, 636–641. https://doi.org/10.1016/j.nimb.2012.07.010.

Tobón, C., Bruijnzeel, L.A., Frumau, K.A., Calvo-Alvarado, J.C., 2010. Changes in soil physical properties after conversion of tropical montane cloud forest to pasture in northern Costa Rica. Tropical montane cloud forests: Science for conservation and management 502–515.

Udom, B., Kamalu, O., 2016. Sealing index, airfilled porosity and hydrological behavior of a tropical Ultisol as affected by incidental flooding and soil disturbance. Int. J. Soil Sci. 11, 79–86. https://doi.org/10.3923/ijss.2016.79.86.

UNSCEAR (United Nation Scientific Committee on the Effects of Atomic Radiation), 1969. United Nations, New York, 24th Session, Suppl. No 13 (A/7613.

UNSCEAR (United Nation Scientific Committee on the Effects of Atomic Radiation), 2000. Sources and Effects of Ionizing Radiation. United Nations Scientific Committee on the Effects of Atomic Radiation. Report to the General Assembly, with Scientific Annexes. United Nations, New York.

Vahabi-Moghaddam, M., Khoshbinfar, S., 2012. Vertical migration of ^{137}Cs in the south caspian soil. Radioprotection 47 (4), 561–573.

Valentin, C., Bresson, L.M., 1997. Soil Crusting. Methods for Assessment of Soil Degradation, pp. 89–107.

Verstraeten, G., Poesen, J., 2000. Estimating trap efficiency of small reservoirs and ponds: methods and implications for the assessment of sediment yield. Prog. Phys. Geogr. 24 (2), 219–251.

Wakiyama, Y., Onda, Y., Mizugaki, S., Asai, H., Hiramatsu, S., 2010. Soil erosion rates on forested mountain hillslopes estimated using ^{137}Cs and ^{210}Pb$_{ex}$. Geoderma 159, 39–52. https://doi.org/10.1016/j.geoderma.2010.06.012.

Walling, D.E., He, Q., Appleby, P.G., 2002. Conversion models for use in soil-erosion, soil-redistribution and sedimentation investigations. In: Handbook for the Assessment of Soil Erosion and Sedimentation Using Environmental Radionuclides. Springer, Dordrecht, pp. 111–164.

Walling, D.E., Zhang, Y., He, Q., 2014. Conversion Models and Related Software, vol. 125. IAEA TECDOC SERIES.

Wang, B., Zheng, F., Römkens, M.J., Darboux, F., 2013. Soil erodibility for water erosion: a perspective and Chinese experiences. Geomorphology 187, 1–10. https://doi.org/10.1016/j.geomorph.2013.01.018.

Watson, R.T., Noble, I.R., Bolin, B., Ravindranath, N.H., Verardo, D.J., Dokken, D.J., 2000. Land Use, Land-Use Change and Forestry: a Special Report of the Intergovernmental Panel on Climate Change. Cambridge University Press.

Wilber, D.N., 1948. Iran, Past and Present. E. L. Hildreth. Company. Brattlebroro Vermont.

Wilken, F., Fiener, P., Ketterer, M., Meusburger, K., Muhindo, D.I., van Oost, K., Doetterl, S., 2021. Assessing soil redistribution of forest and cropland sites in wet tropical Africa using $^{239+240}$Pu fallout radionuclides. SOIL 7 (2), 399–414.

Wischmeier, W.H., Smith, D.D., 1978. Predicting Rainfall Erosion Losses: a Guide to Conservation Planning (No. 537). Department of Agriculture, Science and Education Administration.

Xu, Y., Qiao, J., Hou, X., Pan, S., 2013. Plutonium in soils from northeast China and its potential application for evaluation of soil erosion. Sci. Rep. 3, 3506. https://doi.org/10.1038/srep03506.

Zeraatpisheh, M., Bakhshandeh, E., Hosseini, M., Alavi, S.M., 2020. Assessing the effects of deforestation and intensive agriculture on the soil quality through digital soil mapping. Geoderma 363, 114139. https://doi.org/10.1016/j.geoderma.2019.114139.

Zhang, X., Walling, D.E., Yang, Q., He, X., Wen, Z., Qi, Y., Feng, M., 2006. ^{137}Cs budget during the period of 1960s in a small drainage basin on the Loess Plateau of China. J. Environ. Radioact. 86 (1), 78–91. https://doi.org/10.1016/j.jenvrad.2005.07.007.

Zhang, X.J., Wang, Z.L., 2017. Interrill soil erosion processes on steep slopes. J. Hydrol. 548, 652–664. https://doi.org/10.1016/j.jhydrol.2017.03.046.

Zhang, F., Wang, J., Baskaran, M., Zhong, Q., Wang, Y., Paatero, J., Du, J., 2021. A global dataset of atmospheric ^{7}Be and ^{210}Pb measurements: annual air concentration and depositional flux. Earth Syst. Sci. Data 13 (6), 2963–2994. https://doi.org/10.5194/essd-13-2963-2021, 2021.

Zheng, J., Yamada, M., Wu, F., Liao, H., 2009. Characterization of Pu concentration and its isotopic composition in soils of Gansu in northwestern China. J. Environ. Radioact. 100 (1), 71–75. https://doi.org/10.1016/j.jenvrad.2008.10.017.

Zollinger, B., Alewell, C., Kneisel, C., Meusburger, K., Brandová, D., Kubik, P., Schaller, M., Ketterer, M., Egli, M., 2015. The effect of permafrost on time-split soil erosion using radionuclides (^{137}Cs, $^{239+240}$Pu, meteoric ^{10}Be) and stable isotopes (δ^{13}C) in the eastern Swiss Alps. J. Soils Sediments 15 (6), 1400–1419.